INL/RPT-23-72383-Revision-0

Formation and Consolidation of UN Nanostructures in U-Mo Fuel via Mechanical Alloying and Spark Plasma Sintering

April 2023

James M Zillinger

Changing the World's Energy Future

INL is a U.S. Department of Energy National Laboratory operated by Battelle Energy Alliance, LLC

INL/RPT-23-72383-Revision-0

Formation and Consolidation of UN Nanostructures in U-Mo Fuel via Mechanical Alloying and Spark Plasma Sintering

James M Zillinger

April 2023

Idaho National Laboratory
Idaho Falls, Idaho 83415

http://www.inl.gov

Prepared for the
U.S. Department of Energy
Under DOE Idaho Operations Office
Contract DE-AC07-05ID14517

Formation and Consolidation of UN Nanostructures in U-Mo Fuel via Mechanical Alloying and Spark Plasma Sintering

A Thesis
Presented in Partial Fulfillment of the Requirements for the
Degree of Master of Science
with a
Major in Nuclear Engineering
in the
College of Graduate Studies
University of Idaho
by
James M. Zillinger

Approved by:
Major Professor: Indrajit Charit, Ph.D
Committee Members: Haiyan Zhao, Ph.D.; Samrat Choudhury, Ph.D.; Brian Jaques, Ph.D.
Department Administrator: Indrajit Charit, Ph.D

May 2023

ABSTRACT

Uranium-molybdenum (U-Mo) alloys show promise as a nuclear fuel system due to their high thermal conductivity and high fuel loading capability. However, U-Mo systems suffer from irradiation induced swelling ultimately affecting the cladding via mechanical and chemical interaction. To address these shortcomings, this thesis investigated the formation of uranium mononitride (UN) nanoparticles within a U-10Mo matrix. To promote the formation of UN, U-10Mo powders were mechanically alloyed under a high purity nitrogen cover gas (99.9995%) atmosphere. Variations were made in stainless steel milling media size, duration of milling, and number of times the milling jar was re-aerated with nitrogen gas. UN nanoparticulates were successfully formed within the U-Mo matrix and was characterized utilizing light element analysis, X-ray diffractometry, scanning and transmission-electron microscopy, electron energy loss spectroscopy, and atom probe tomography. Presence of the UN nanoparticles was found as early as 1-hour into the mechanical alloying process, and significant iron contamination found after 10-hours of milling. The U-Mo/UN powders were compacted using spark plasma sintering techniques in order to stabilize the nanostructure. U-Mo/UN compacts containing small amounts of neodymium and helium were analyzed to observe the defect migration tendencies of fission products within the fuel.

ACKNOWLEDGEMENTS

I am indebted to Dr.'s Nathan Jerred, Indrajit Charit, and Samrat Choudhury for their allowance of me to work on this project, as well as their constant feedback, guidance, and patience as I performed the hands-on-research. They took a lot of time out of their schedules to support me as I needed direction for parameterization for the project, and for the writing of this thesis.

This work was supported through the INL Laboratory Directed Research & Development (LDRD) Program under DOE Idaho Operations Office Contract DE-AC07-05ID14517.

Additional thanks to Kevin Tolman, Fidelma DiLemma, Tiankai Yao, Mukesh Bachhav, Fei Teng, and Trishelle Copeland-Johnson, for technical assistance and guidance during this work.

I extend my sincere gratitude to the U170 and U110 organizations at the Materials and Fuels Complex (MFC), with specification to Adrian Wagner and Jennifer Watkins for their guidance and expertise in the uranium nitride system and planetary milling. Additionally, I wish to personally thank Randall Scott for his dedication to helping me spark plasma sinter this material and fixing the DCS-50 on multiple occasions.

DEDICATION

I would like to dedicate this thesis to my late mother, Kathleen Zillinger, and father, Charles Zillinger who showed saint-like love and patience for me all through my youth and young-adult years. Without their rearing and guidance, I most certainly would not be the man I am today, or likely have proceeded to such a point in my education.

Additionally, I am ever grateful to my fiancé, Melody, who has continuously supported my time spent furthering my education and inspired me to persevere. I hope this knowledge attained may be used to further bless my career in supporting her and our family.

I am very thankful to my teachers at Troy High School for putting me on this path in the first place, namely Mr. Bruns for his teaching of science and acting as a source of inspiration for me to become a nuclear engineer. I also wish to thank my undergraduate professors in Materials Science and Engineering for their time dedicated both in and out of the classroom to help me get the most out of my bachelor's degree.

Finally, I wish to thank God for his unending blessings to me. I pray my intellect may be used to His service, and I may never take the wonderful gifts and opportunities that I have received for granted. To God be the glory for any good that comes from this research.

TABLE OF CONTENTS

LIST OF FIGURES

LIST OF TABLES

DISCLAIMER

CHAPTER 1
Introduction

1.1 Background & Motivation

Numerous efforts to address the fuel-cladding interactions have been made in the past two decades through the Reduced Enrichment for Research and Test Reactors (RERTR) program and other parallel initiatives. Use of dopants, different cladding materials, reduced fuel smear density, and varying fuel geometries have been investigated with varying degrees of success [1-8]. The primary method for combatting fuel-cladding interactions was the reduction in smear density to a commonly accepted 75%. This provided adequate room for swelling in the fuel as burnup increased. This was tested within the Integral Fast Reactor's (IFR) U-10Zr fuel supply in the 1960's, and high burnups (~20%) were achieved. For Gen IV reactors to achieve even higher burnups (40-60%) current innovations are considering even lower fuel smear densities. While the reduction of smear density, addition of dopants to immobilize fission products, and implementation of liners allow for theoretically greater burnups, it also poses the issue of shorter intervals between fuel changeout due to a lower total mass of fissile material in the system.

Ferritic steels have utilized dispersed nanometric oxides to improve performance in structural materials in a variety of ways. An improvement relative to the issue of swelling mentioned in the previous paragraph, is the attraction of helium to the interface regions between the steel and oxide nanoclusters. Once the helium diffuses to the interface region, it will reside within the interstitial spacing of the oxide's lattice spaces, which prevents the formation of large-scale porosity within the steel. This work's primary purpose was to prove that this phenomenon was not limited to a ferritic system, and nanostructuring of a metallic fuel system could be achieved through mechanical alloying in a high purity gas overfill setup. If successful, this could allow for swelling reduction in the U-Mo system without the need to reduce smear density or add in non-fuel dopants for fuel survival.

This research was conducted in conjunction between the Idaho National Laboratory (INL) and two university partners, University of Idaho, and University of Mississippi. The

inspiration for this work came from Dr's. Choudhury and Charit and has been several years in the making with regard to background research, theoretical feasibility studies, and related research from previous students at the University of Idaho. The primary motivation of this work was to address a major drawback in the uranium-molybdenum fuel system, which is the fuel-cladding interactions that occur at higher burnups, due to swelling in metallic fuel systems.

1.2 Objectives

The overall objective of this research was to demonstrate the proof-of-concept of a novel nanostructured metallic fuel using nanosized uranium mononitride (UN) particles embedded within a uranium-molybdenum (U-Mo) metallic matrix as a model system. This fuel has the potential to significantly reduce chemical interactions at the fuel-cladding interface and swelling compared to monolithic U-Mo metallic fuel.

The proposed method for creating the nanosized UN particles was through milling, in which U-10Mo powder would be placed into a mill-jar pressurized with high purity nitrogen and shaken rapidly. This shaking motion causes the milling media inside the jar to collide with one another, and, if there is U-Mo in-between two of the balls when they collide, it will create a localized high temperature region, in which the nitrogen gas can be driven into the fuel through a cold-welding process. Through this repeated localized alloying, the goal was to create a homogenously distributed UN nanostructure across the U-Mo matrix.

The specific phase of uranium nitride is hypothesized to be due to the partial pressure of nitrogen present within the system, leading to a UN phase with a lower total amount of nitrogen introduced into the system, and a uranium dinitride (UN_2) or uranium sesquinitride (U_2N_3) phase developing with greater amounts of nitrogen introduced. The kinetics of this reaction are presumed to be near-instantaneous, but a heat-treatment would be conducted to stabilize a nitride phase in case the cold-working only imbedded nitrogen atoms into interstitial spacing.

These nanostructures were to be characterized and the verification of phase, size, stability, and homogeneity were the key data points obtained for this thesis.

1.3 Thesis Outline

This thesis is summarized across five chapters in total, with the general following topics: Chapter 1: Introduction to research, Chapter 2: Background literature, Chapter 3: Overview of feedstock U-10Mo production and qualification, Chapter 4: Research in UN formation through mechanical alloying, and stability after sintering and heat-treatment, and Chapter 5: Conclusions and future plans. Chapters three and four will have their own introductions, materials & methods, results & discussion, and conclusions, and each chapter will have a separate bibliography.

1.4 References

[1] A. Wright, S. L. Hayes, T. H. Bauer, H. Chichester, G. Hofman, J. R. Kennedy, T. K. Kim, Y. S. Kim, R. Mariani, W. Pointer, A. Yacout, and d. Yun, "Development of advanced ultra-high burnup SFR metallic fuel concept - Project overview," *Transactions of the American Nuclear Society,* vol. 106, pp. 1102-1105, 01/01 2012.

[2] W. Zhuo, Y. Xie, M. T. Benson, H. Wu, R. D. Mariani, and J. Zhang, "Experimental assessment of antimony (Sb) in pure uranium for immobilizing fission product lanthanides," *J Nucl Mater,* vol. 534, p. 152135, 2020/06/01/ 2020, doi: https://doi.org/10.1016/j.jnucmat.2020.152135.

[3] Y. Xie and M. T. Benson, "Microstructure and diffusion behavior of uranium fuel with minor additives," *J Nucl Mater,* vol. 535, p. 152200, 2020/07/01/ 2020, doi: https://doi.org/10.1016/j.jnucmat.2020.152200.

[4] R. Khanal, N. Jerred, M. T. Benson, Y. Xie, R. D. Mariani, I. Charit, and S. Choudhury, "Interactions and immobilization of lanthanides with dopants in uranium-based metallic fuels," *J Nucl Mater,* vol. 540, p. 152372, 2020/11/01/ 2020, doi: https://doi.org/10.1016/j.jnucmat.2020.152372.

[5] R. Khanal, N. Jerred, M. T. Benson, D. A. Andersson, R. D. Mariani, I. Charit, and S. Choudhury, "A novel approach to selection of dopant to immobilize neodymium in uranium-based metallic fuels," *J Nucl Mater,* vol. 529, p. 151922, 2020/02/01/ 2020, doi: https://doi.org/10.1016/j.jnucmat.2019.151922.

[6] N. D. Jerred, R. Khanal, M. T. Benson, E. Perez, J. A. King, M. Dubey, J. Burns, I. Charit, S. Choudhury, and R. D. Mariani, "Evaluation of Tellurium as a Fuel Additive in Neodymium-Containing U-Zr Metallic Fuel," *Scientific Reports,* vol. 9, no. 1, p. 16043, 2019/11/05 2019, doi: 10.1038/s41598-019-51852-z.

[7] Y. Xie, J. Zhang, M. T. Benson, and R. D. Mariani, "Diffusion behavior of lanthanide-additive compounds (Ce4Sb3, Ce2Sb, and CeTe) against HT9 and Fe," *Materials Characterization,* vol. 150, pp. 107-117, 2019/04/01/ 2019, doi: https://doi.org/10.1016/j.matchar.2019.02.012.

[8] Y. Xie, J. Zhang, M. T. Benson, J. A. King, and R. D. Mariani, "Assessment of Te as a U-Zr fuel additive to mitigate fuel-cladding chemical interactions," *J Nucl Mater,* vol. 513, pp. 175-184, 2019/01/01/ 2019, doi: https://doi.org/10.1016/j.jnucmat.2018.10.050.

CHAPTER 2

Literature Survey

Uranium-molybdenum (U-Mo) alloys are a candidate fuel for next generation fast-reactors because of their attractive thermal conductivity and high fuel loading potential. However, this fuel system is inhibited by major swelling during operation, as well as both chemical and mechanical interaction with the traditional aluminum cladding [1]. To address these shortcomings, this work was conducted to form an interspersed uranium mononitride (UN) phase within a U-10 wt% Mo (U-10Mo) alloy that can act as defect annihilation sites and increase overall fuel performance. The method for forming this phase is similar to that of oxide dispersions strengthening (ODS) of various alloys in the past. ODS alloys have been of interest in the nuclear energy world as early as the 1970's, with offerings of increased creep resistance, increased strength at high temperatures, and reduction to alloy swelling [2]. While ODS is primarily implemented into alloy steels for structural components within reactors, all of these properties are also desirable within the U-Mo fuel system. ODS alloys are typically created through a mechanical alloying process in which a powder form of the alloy is milled at high energies with minute quantities of yttria or other oxides to create nanometric oxide particulates within the material [2-6]. In recent years, a similar method of mechanical alloying has been developed for forming nitrides. Instead of a nitride addition, however, metallic alloys are simply milled under a nitrogen atmosphere [7-12]. Ferrous nitrides, TiN, Mo_2N, and U_2N_3 have been formed via this method [13]. These methods typically include high energy milling techniques operating between 1100-1700 rpm [4, 5] to mechanically embed the desired phase for good dispersion strengthening. Reasons for pursuing nitrogen milled alloys ranged from increased strength and electrical conductivity to corrosion resistance and improved toughness in the alloys. References typically used stainless steel milling media, but some utilized yttria-stabilized zirconia, as it is a much harder material, and results in less contamination (Fe, Cr, etc.) within the system. Varying ball-to-powder ratios were noted in literature, and a 10:1 ball to powder (BTP) weight ratio was typical amongst most studies.

2.1 U-Mo Alloy Properties

The U-Mo alloy system has been a studied fuel system for nuclear reactors since at least 1944 as outlined by IAEA and Ahmann et al. [14, 15]. Currently, U-Mo is a primary fuel for research reactors and candidate for next generation fast reactors [1, 16]. Primary advantages to this system are its high-fuel loading, low parasitic neutron absorption, and stabilized BCC crystal structure (γ-phase) between the 6-10 wt% (~13.7-21.6 at%) additions of molybdenum (Mo), as can be seen in the phase diagram in Figure 2.1.

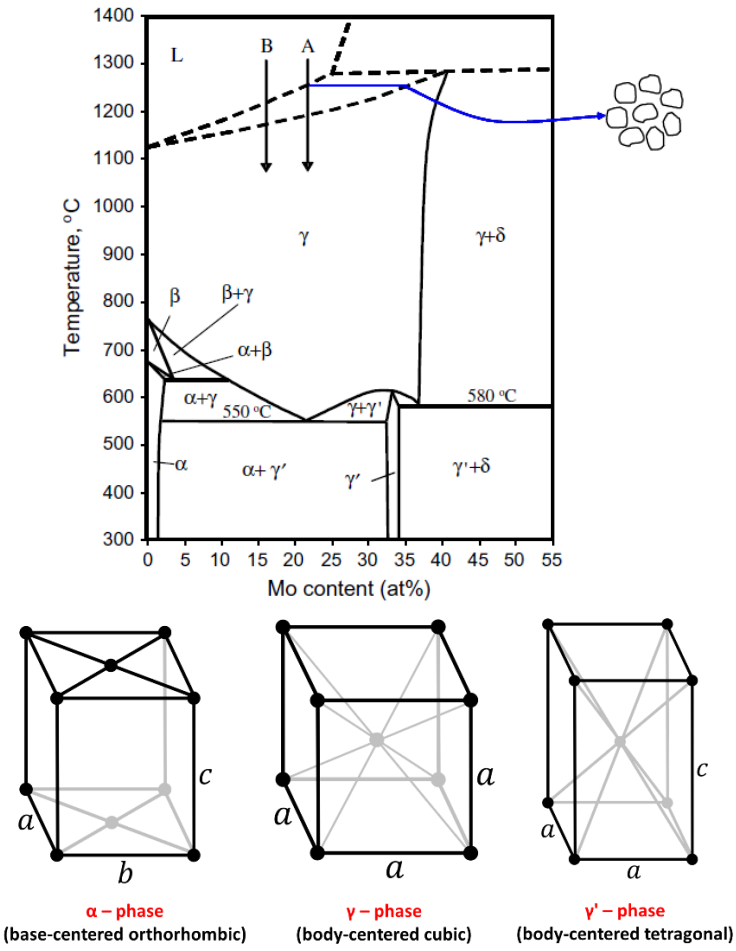

Figure 2.1: (Above) Partial phase diagram showing the different solid phases present in the U-Mo system. Note eutectoid region ~22 at% resulting in the most stable form of the BCC γ-phase, U-10Mo [17]. (Below) Visualized phases of U-Mo alloys [18].

Stabilizing the BCC structure within a metallic fuel is advantageous due to its isotropic swelling behavior in addition to having a greater number of interstitial defect sites that can contain gaseous fission products such as Xe, I, and Kr [17]. Unlike α and γ' phase, the cubic crystal structure is isotropic, allowing of even expansion of crystals in all directions. The

greater number of interstitial sites in a cubic crystal is beneficial in the total reduction of swelling within the fuel and allows for longer time periods of fuel operation before formation of macroscopic voids and subsequent interconnected porosity leading to gas diffusion into the plenum. Fuel swelling is the driving factor behind fuel-cladding mechanical interaction (FCMI), as the expansion due to formed fission products cause the fuel to contact cladding radially. The accepted equation used to describe the combined effect of both solid and gaseous fission products is shown in the following equation [1].

$$\left(\frac{\Delta V}{V_0}\right)_{total}(\%) = \left(\frac{\Delta V}{V_0}\right)_{gaseous} + \left(\frac{\Delta V}{V_0}\right)_{solid} \tag{2.1}$$

ΔV is the V_{final}-V_0 which are the final and initial volumes of the fuel respectively, and the gaseous and solid volume changes are from their respective solid and gaseous fission products. For solid products,

$$\left(\frac{\Delta V}{V}\right)_s = 3.5 * 10^{-21} f_d \tag{2.2}$$

and f_d is fission density in units of fissions/cm^3. The rate of swelling due to solid fission products acts as a linear function of burnup. In gases, however, the swelling changes exponentially as a function of burnup.

$$\left(\frac{\Delta V}{V}\right)_g = f_d * (1.8 * 10^{-21}) \ \ at\ f_d \leq 3 * 10^{21}\ fissions/cm, \tag{2.3}$$

$$\left(\frac{\Delta V}{V}\right)_g = 5.4 + (2.1 * 10^{-21})\ (f_d - 3 * 10^{21}) + 0.43 * 10^{-42}(f_d - 3 * 10^{-21})^2 \quad at\ f_d \geq 3 * 10^{21}\ fissions/cm^3 \tag{2.4}$$

Based on these, the swelling will increase exponentially with time as shown by Figure 2.2 from the U-Mo fuels handbook.

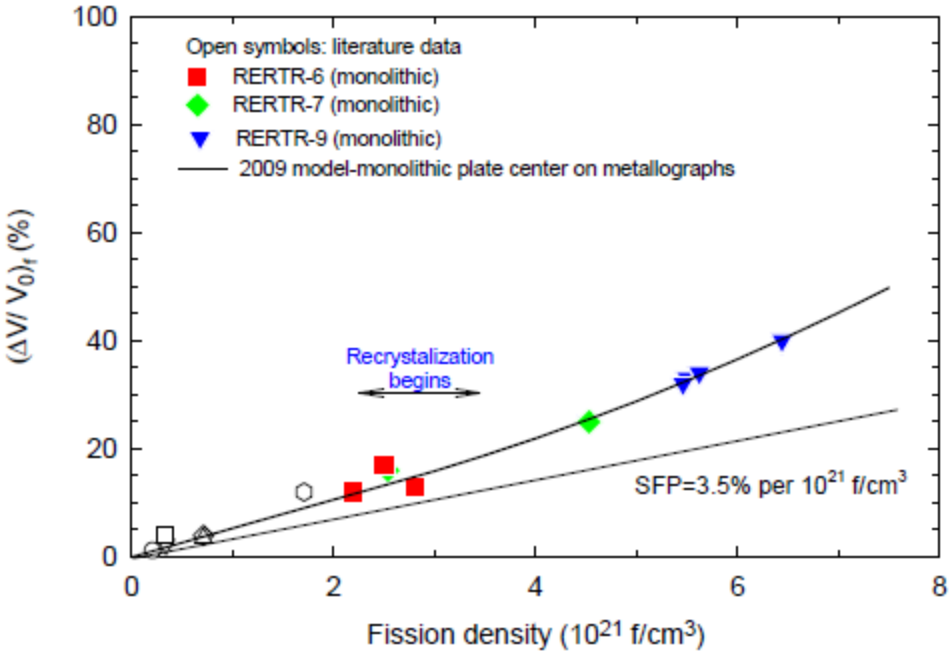

Figure 2.2: Measured vs. calculated swelling behavior in monolithic U-10Mo fuel [1]. SFP= solid fission products

This is seen across different compositions of U-Mo fuels, but the effects of swelling are minimized at the U-10Mo composition, due to its limited ability to form either α or γ' phases at elevated temperatures (Reference Figure 2.1 at the eutectoid temperature and Figure 2.3 for swelling rates).

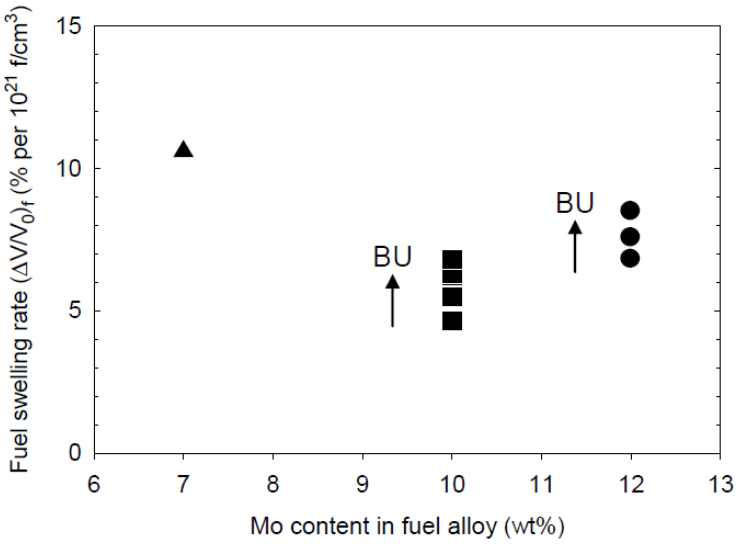

Figure 2.3: Effects of Mo content on swelling in U-Mo alloys [1] Burnup (BU) also increases swelling shown in the 10 and 12 wt% Mo alloys

The U-Mo system's limited disassociation into the α or γ' phases is a favorable mark on the U-Mo alloy's record, as U-Zr fuels will commonly form a two-phase system when at elevated temperatures for long periods of time.

If enough swelling occurs, the cladding may rupture. This has been addressed in the past by reducing smear density in the fuel to account for swelling, but due to fission products accumulating at porosity sites and reducing open space for swelling to occur, even this does not fully solve the issue of FCMI. Imposed burnup limits are a design engineer's main methods of preventing this interaction in the field, but this still prevents metallic fuels such as U-Zr and U-Mo from reaching their true potential.[19]

A related complication in U-Mo and other metallic fuel systems is the interaction of solid fission products with fuel cladding. Solid fission products are primarily made up of lanthanides (La, Nd, Ce, etc.), which form their own secondary precipitates as burnup increases during reactor life. Figure 2.4 shows that lanthanides formed near the edge of the fuel that contact the cladding often form low melting point eutectics that can also cause cladding failure in strained circumstances.

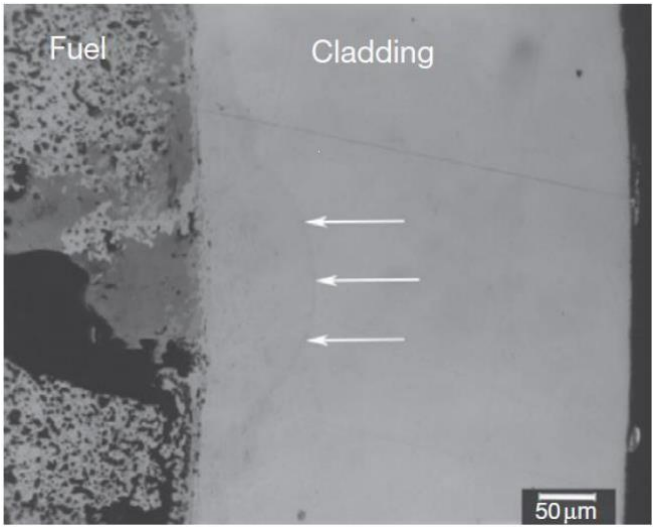

Figure 2.4: Solid fission product interaction layer with cladding [20]

Lanthanide interaction with the cladding is exaggerated by the effects of solid state diffusion in the fuel driven by temperature gradients, neutron irradiation, and phase transformation [19, 20]. This phenomenon is known as fuel-cladding chemical interaction (FCCI) and is one of the primary limiters to burnup life in U-Mo and other metallic fuel systems alike.

Methods have been developed over the last decades to try and address FCMI and FCCI within metallic fuel systems. Some methods include the addition of dopants to form intermetallic bonds with lanthanides, alloying additions to impede insoluble phase migration, gas vent design for plenum pressure relief, and lining of the inner cladding wall with a compatible material such as chromium, zirconium, or vanadium [21-29]. Dopants added to the fuel are chosen based on lanthanide affinity to form compounds within the metal fuel alloy, but not interact with uranium. Limited success has been achieved with the addition of dopants or alloying additions to the fuel, as it is difficult to reproduce the conditions undergone by fuel in a reactor. Examples include: The temperature gradient going from a high to low from the centerline to circumference of the fuel pins, long time periods at fluxuated elevated temperatures, and neutron irradiation effects. In typical heat-treatment experiments, diffusion of the solid fission products did not occur to the same extent as observed in post-irradiated fuel pins removed from reactors. To account for the differences, researchers have made up for it by increasing heat-treatment temperatures and dwell times to reach thermodynamic equilibriums in realistic timeframes.

In terms of benefits seen in the U-Mo system, thermal conductivity is a major boon, as it is much more conductive and has less heat capacity than ceramic fuel competitors, making it easier to cool, or remove heat from in case of emergency. A comparison of conductivities and heat capacities in some common fuels are shown in Table 2.1 for reader comparison.

Table 2-1: Thermal heat capacity and conductivity data for Various Nuclear Fuels

Fuel Type	**Heat Capacity J/(kg*K) @ 500 ˚C**	**Thermal Conductivity W/(m*K) @500 ˚C**	**Melting Point K @ 1 atm**
U [30-32]	40.93	33.5	1,132 ˚C
U-10Mo [1]	38.3	27.6	~1,150 ˚C
U-10Zr [33]	35	27.5	1,250 ˚C
UO_2[34, 35]	307	4.1	2,865 ˚C
UN [36, 37]	57.35	20.7	2,850 ˚C
UC [36, 38]	50.11	19.5	2,350 ˚C

It is shown that metallic fuels carry a lower heat capacity, while having a much larger thermal conductivity than traditional UO_2, and marginally more than UN and UC. Comparatively to pure metallic uranium, thermal conductivity of the alloyed U-Mo and U-Zr is lower, which is a price paid for the retained metastable gamma phase.

Gamma and neutron irradiation also effects U-Mo fuel systems in significant ways. As burnup increases, the thermal conductivity of the fuel decreases due to increased void formation and presence of dissimilar fission products. This is explained via the Bruggeman method, and details may be found in the U-Mo fuels handbook [1]. Irradiation will also cause the breakdown of the gamma phase into its respective tetragonal and orthorhombic constituents if the operating temperature is below 565 ˚C. Operation above the aforementioned temperature allows for a constant restabilizing effect on the BCC structure. As the molybdenum content is raised, the transformation from γ to $\alpha+\gamma$ is noted to significantly reduce.

Regarding physical advantages of U-Mo fuel, it is easily formable into complex geometries, like foils, plates, and cast ingots. By the easy method of alloying uranium and molybdenum by melting and quenching, it opens the door for more exotic reactor fuel types than the

traditional pellet stack up. One such example includes the advanced test reactor at the Idaho National Laboratory, which has its uranium-aluminum plates in a unique “four leafed clover” type shape.

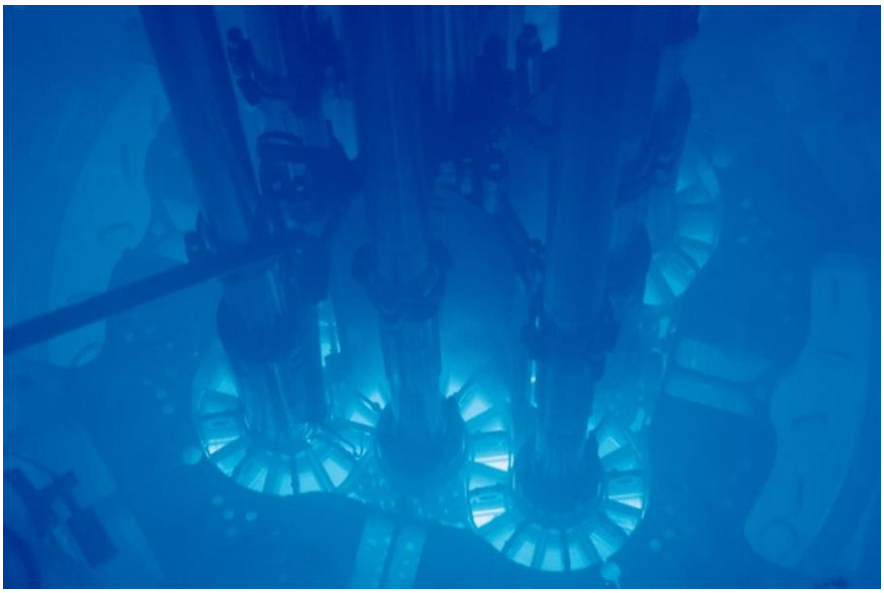

Figure 2.5: Photograph taken of the ATR and its unique fuel geometry compliment to the INL [39].

The development of metallic fuel in varying geometries is of particular interest in fast reactor development. U-Mo alloys fit well as a fast reactor fuel due to its high heavy metal content, simpler phase structure than U-Zr, and higher thermal conductivity, according to Kim et al [16]. Again, the swelling is the primary downside to U-Mo fuel, but next generation reactor designers are willing to utilize lesser smear densities (typically ≤75%), adequate plenums/fission gas venting systems, and thicker cladding to prevent rupture from swelling until a time comes that fuels may be developed that removes the need for swelling inhibitors. Additional interest lies in changing the cladding utilized with U-Mo. Aluminum has historically been used as the cladding material for U-Mo fuels, but with fast reactors not having the same concerns for hydrogen buildup that BWR’s and PWR’s have due to zircaloys interaction with steam, the idea of using the zirconium based cladding materials for fast reactors has also been suggested in Kim et al.’s publications [16, 21]. Additional materials include different types of ferritic alloys, like Fe-Cr-Al, to be used, but little in depth research on U-Mo interactions with these claddings, or with the coolant salts has been conducted for these claddings.

Finally, a major advantage of the U-Mo fuel system and metallic fuel systems as a whole, is the ease at which fuel can be recycled [40]. During the operation of EBR-II, U-Zr spent fuel was removed from the reactor and sectioned into small pieces. The fuel was then separated from the salt via electro-refining process and was put into a furnace and raised to the fuel's melting temperature. The remaining insoluble lanthanides rose to the top and could be skimmed off if needed, leaving a bulk U-Pu-Zr fuel leftover for refabrication into fuel pins and re-insertion into the reactor. While the USA does not currently recycle fuel due to non-proliferation agreements with foreign countries, having the ability to recycle spent fuel should the need ever arise is smart, especially considering spent fuel is stored on-site at reactor locations nationwide until a national repository is designated.

2.2 Hydride-Dehydride of U-10Mo

In order to expedite the initial U-10Mo feedstock production for ready availability, it was proposed to investigate the hydride-dehydride (HDH) process in U-Mo alloys. Substantial amounts of unusable material (30-50% process loss) as well as large particle size (150-250 micron) dedicated to the pursuit of other powder production avenues. Higher quantities of powders could be made per batch if HDH was successful. In addition, a theoretically smaller particle size (<50-150 μm) [41, 42] could be reached.

In Chen et al's publication [41], HMDH powders had reported particle sizes of "...less than 50 μm.", in addition to retaining the original gamma phase crystal structure after the final dehydriding process. X-Ray Diffraction (XRD) patterns did not show residual hydrides remaining after dehydriding, and maximum hydrogen saturation of the U-10Mo (0.8577 mL of H/ g of U-10Mo) was seen after eight cycles. Mass of U-10Mo powder was not provided to compare hydrogen absorption level to. Unique factors of this study include that the U-10Mo powders were not put under a long heat treatment to transform the gamma to an alpha phase before the HMDH process took place.

In Xiong Yi-Fu et al's publication [43] the heat treatment process was noteworthy, as it claimed the gamma phase U-Mo "exhibits metallic ductility and cannot be easily reduced to powder via grinding…". Their HDH process consisted of cleaning the sample, followed by placement within the reactor, raising the temperature to 250 ℃ at a rate of 5 ℃/s to cook off impurities. Finally, the sample dropped to room temperature, and the reactor was pressurized

to 4-5 atm H_2. It was specified that hydrogen absorption was monitored via pressure transducer and a connected computer and was stopped when absorption reached a plateau. The dehydride process followed by heating the reactor + sample to 600 C at 5 ℃/s. This publication was important as the authors were able to achieve 100-150 µm particulate size without a milling step incorporated in the HDH process. 10 HDH cycles were used to obtain this powder size.

In Durazzo et al's paper [42] a cast U-10Mo rod was created from stock material, then heat treated at 1000 ℃ for 72 hours under argon, and cooled to retain the gamma phase [42]. Using a hydride-mill-dehydride route, smaller samples were taken off the rod, and heated to 400 ℃ for 3 hours under high purity hydrogen at 3 bar. They did not expect or see an alpha phase transformation take place during this process based off a referenced [44] TTT diagram. The hydride pieces were initially crushed using a stainless-steel mortar. U-Mo granules (~3 mm in length) were then milled in a planetary mill at 400 rpm for 10 hours with BTP ratio of 20:1 using hardened steel balls and vial. After milling, the powders were heat treated under vacuum at 400 ℃ do dehydrogenize. Mean particle size was 100 µm and number of cycles was not noted within the experiment.

Within a publication by Vaz de Oliveira [45], U-Mo alloys varying in composition from U-5Mo to U-10Mo were put through a hydration cycling, and breakup was observed. Powder formation mechanisms were explored in depth, and it was experimentally found that fragmentation did occur in U-9Mo and U-10Mo alloys. This was presumed to be due to the overall fraction of α-U phase to that of the γ-U phase, which becomes so low at 9-10 wt% Mo that powder breakup was not feasible. This implies a maximum stability is reached in the U-Mo system above 9 wt% Mo. This provided a contrary view to the suppositions found in the previous papers on the hydride-dehydride of U-10Mo.

In a publication by Steiner et al. [46], the transformation mechanisms of γ-phase to α-phase in the U-Mo system was explored. The authors explained that in molybdenum lean U-Mo alloys, α-phase would be present in higher quantities and the eutectoid decomposition would be more readily reached. It also talks to the precise range of temperatures needed to be reached in order to form the partial alpha phase that "decorates" the γ-U phase, which for the U-8Mo system falls between 467 ℃ and 542 ℃ temperature band. The highest rate of change

from γ-phase to α-phase was seen for this system at 498 ℃. Data on lattice parameter relation as a function of α-content, as well as kinetics relationships were all analyzed within the paper. This data was used to compare behavior in the U-10Mo to that of the U-8Mo system and draw connections to the current U-10Mo system.

2.3 Milling Parameters – ODS Inspiration

Oxide dispersion strengthening (ODS) has been implemented as a vital nuclear reactor technology for about twenty years. ODS is the inclusion of oxide nanoprecipitates in a metallic alloy that provide numerous benefits such as swelling reduction, and increased strength and creep resistance. In more conventional alloys, helium gas is a typical candidate for swelling as it will create macro-pores and voids. With nanometric oxides incorporated, however, the helium will preferentially aggregate in and around the nano-oxides, which prevents larger pore formation [2].

While little information was found on the mechanical alloying of U-Mo systems [1], there are several newer publications investigating the oxidation/nitriding of steel, titanium, and zirconium using ball milling techniques. In Calka's publication [8], he used an in-house made ball mill to create titanium and zirconium nitrides under a constant nitrogen gas pressure during milling. Past successfully creating TiN and ZrN, Calka calculated grain sizes of these nitrides to be 9 nm (for TiN) and 14 nm (for ZrN) using Scherrer's formula. Mechanical alloying was conducted in 99.99% N_2 gas at 12-, 36-, 40-, 60-, and 120-hour intervals, and an annealing process was performed for both TiN and ZrN specimens afterwards to "determine the single-phase structure of the as-milled powder…". Other milling parameters were not provided save for initial particle size of powder being between 100-200 μm, and the use of stainless-steel balls as milling media.

Calka [8] also made considerable mention of particle surface roughness' effect on nitrogen absorption in this system. He stated rough metal surfaces would see far less nitrogen dissociation than smooth surfaces, and that nitrogen absorption and adsorption rates could be greatly increased above 400℃. No mention of iron contamination was mentioned within Calka's work.

In a similar study by C. Duan et al. [7] the authors used a Fritsch Pulverisette 6 planetary mill to create nanometric nitrides within steel. More detailed process parameters were given in

this paper, explaining that nitrides were formed by milling the alloy powder at 350 rpm with stainless steel media in 10:1 ball to powder ratio for 10-, 15-, 20-, and 25-hour timeframes. Initial steel powder size was 13.96 μm, and after the maximum mill time of 25 hours decreased to 7.96 μm.

In an article by J.J. Park et al. [4], a planetary mill was used to create ODS alloys, but was ran at very high disk speeds (1100 rpm). These Fe powders were milled for 10 and 90 minutes before being sintered using spark plasma sintering (SPS) techniques. Using XRD and transmission electron microscopy (TEM) techniques, Park et al. was able to verify nanophase yttria particles in the ferrous matrix. Again, stainless steel was used for the milling media (8 mm diameter), but the ball: powder ratio was 20: 1 in this case. The author emphasizes the use of 50–60-micron course yttria particulates as the starting powder (along with similar sized Fe and Cr powders). Decline in yttria XRD peaks were seen readily after 10 minutes of milling, and post sintered samples showed the yttria reformed with Cr to make $YCrO_3$.

In Pasebani's dissertation [47], it was stated that a SPEX 800M high energy ball mill was used at 1725 rpm to alloy the powder. Stainless steel ball media (diameter = 5 and 8 mm) was used in a 10:1 ball to powder ratio, and mechanical alloying was conducted for 2-,5- ,10- ,15- and 20-hour time ranges. Pasebani also tried milling runs using a mix of media both 5 and 8 mm in diameter, resulting in the smallest crystallite size, but a larger overall mean particle size. (Table 3.4 in dissertation).

In research by Murty and Ranganathan [6], the effects of milling time and temperature on milled nickel and iron based ODS powders were referenced. Key points mentioned were the amorphization of milled powders over long mill times (30 to 40 hours), and the widely used ball/powder weight ratios of 5:1 – 10:1. It also states that since high energy milling is characterized by repeated welding and fracture of the powder, that phase transition during milling is primarily a function of milling temperature. In regard to media material, it states that Fe contamination could be a "blessing in disguise" as it produced completely disordered nanocrystalline materials, while tungsten carbide (WC), and carbon steel (CS) have produced partially ordered forms of nanocrystallites instead. Other publications claim this disorderly arrangement could increase ductility within the alloy [48, 49]. Additionally, in an

unpublished study on Cu-Ni mechanical alloying mentioned in Murty and Ranganathan's publication, chrome steel, stainless steel, and tungsten carbide media were used to mill separate powders for 20 hours [6]. The CS and SS media samples successfully alloyed the Cu and Ni, but the WC media sample failed to form a solid solution. This was attributed once more to Fe contamination.

Based on Park's work [50], it should be possible to form nanometric nitrides in a shorter timeframe than mentioned in other papers (1-5 hours instead of 12-120) as long as milling operations are performed at high rpms (2640 rpm). Using steel media may be an issue in this case if Fe contamination is of concern, as the increased milling intensity will degrade the media at an increased rate. On the other hand, Murty and Ranganthan [6] stated that Fe contamination could actually help in the alloying process; the alloying between U-Mo will take place beforehand via arc melting, meaning there wouldn't be a concern of not forming a solid solution. Using a WC lined jar and mill media at high intensities would seem to be the best route for quick turnaround of nitriding results with smaller risk of fuel contamination. If longer milling times were acceptable for this work, and desire to follow the bulk of literature was priority; stainless steel media would work best, in addition to reducing variance from previous mechanical alloying research. A ball to powder ratio of 10:1 would be a safe starting point, as mentioned in previous literature. Additionally, using media diameter of varying diameters (3, 5, and 8 mm) are recommended in order to optimize end powder size and hopefully surface roughness.

2.4 Effects of Iron in Uranium Alloys

Considering the risk of iron contamination within the U-10Mo fuel meat was a real concern if stainless steel was used as the milling media, a short review was conducted on the effects of iron in uranium. In Chatain et al.'s report [51], it is confirmed that uranium and iron form two low melting point eutectics, U_6Fe at 720.85 ℃ and UFe_2 at 1076.85 ℃. A concerning factor is that only a small amount of iron (3.7 wt%) is necessary to induce a partial melt within a uranium fuel body.

2.5 References

[1] J. Rest and Y. S. H. Kim, G.L. Meyer, M.K. Hayes, S.L. A. N. Laboratory. (2006). U-Mo Fuels Handbook.

[2] D. T. Hoelzer, "History and Outlook of ODS/NFA Ferritic Alloys for Nuclear Applications," *Transactions of the American Nuclear Society,* vol. 118, p. 4, June 17-21, 2018 2018.

[3] C.-L. Chen and C.-L. Huang, "The effects of alloying and milling on the formation of intermetallics in ODS tungsten heavy alloys," *Intermetallics,* vol. 41, pp. 10-15, 2013, doi: 10.1016/j.intermet.2013.04.014.

[4] J. J. Park, S. M. Hong, E. K. Park, M. K. Lee, and C. M. Rhee, "Synthesis of Fe based ODS alloys by a very high speed planetary milling process," (in English), *J Nucl Mater,* vol. 428, no. 1-3, pp. 35-39, Sep 2012, doi: 10.1016/j.jnucmat.2011.12.027.

[5] S. Pasebani, "Processing of Oxide Dispersion Strengthened Alloys via Mechanical Alloying and Spark Plasma Sintering," PhD, Materials Science and Engineering, Materials Science and Engineering, University of Idaho, 2014.

[6] B. S. Murty and S. Ranganathan, "Novel materials synthesis by mechanical alloying/milling," *International Materials Reviews,* vol. 43, no. 3, pp. 101-141, 2013, doi: 10.1179/imr.1998.43.3.101.

[7] C. Duan, Y. Shen, X. Feng, C. Chen, and J. Zhang, "Nitriding of Fe–18Cr–11Mn powders using mechanical alloying method through aerating nitrogen circularly," *Materials Science and Technology,* vol. 32, no. 12, pp. 1231-1239, 2016, doi: 10.1080/02670836.2015.1115244.

[8] A. Calka, "Formation of titanium and zirconium nitrides by mechanical alloying," *Applied Physics Letters,* vol. 59, no. 13, pp. 1568-1569, 1991, doi: 10.1063/1.106285.

[9] M. M. Cisneros, H. F. Lopez, H. Mancha, D. Vazquez, E. Valdes, G. Mendoza, and M. Mendez, "Development of austenitic nanostructures in high-nitrogen steel powders processed by mechanical alloying," (in English), *Metall Mater Trans A,* vol. 33, no. 7, pp. 2139-2144, Jul 2002, doi: DOI 10.1007/s11661-002-0045-1.

[10] T. Haghir, M. H. Abbasi, M. A. Golozar, and M. Panjepour, "Investigation of alpha to gamma transformation in the production of a nanostructured high-nitrogen austenitic stainless steel powder via mechanical alloying," (in English), *Mat Sci Eng a-Struct,* vol. 507, no. 1-2, pp. 144-148, May 15 2009, doi: 10.1016/j.msea.2008.12.033.

[11] W. Y. Lim, M. Hida, A. Sakakibara, T. Takemoto, and S. Yokomizo, "Structural Stability and Mechanochemical Activity of Titanium Nitride Prepared by Mechanical Alloying," (in English), *J Mater Sci,* vol. 28, no. 13, pp. 3463-3466, Jul 1 1993, doi: 10.1007/Bf01159823.

[12] I. Lucks, P. Lamparter, and E. J. Mittemeijer, "Uptake of iron, oxygen and nitrogen in molybdenum during ball milling," (in English), *Acta Mater,* vol. 49, no. 13, pp. 2419-2428, Aug 1 2001, doi: 10.1016/S1359-6454(01)00154-9.

[13] B. J. Jaques, B. M. Marx, A. S. Hamdy, and D. P. Butt, "Synthesis of uranium nitride by a mechanically induced gas-solid reaction," *J Nucl Mater,* vol. 381, no. 3, pp. 309-311, 2008/11/15/ 2008, doi: https://doi.org/10.1016/j.jnucmat.2008.07.043.

[14] D. Ahmann, A. I. Snow, and A. S. Wilson, "THE URANIUM-MOLYBDENUM BINARY SYSTEM," vol. 12-B, ed: OSTI, 1945, p. 28.

[15] P. A. Adelfang, N; Dobrikova, I.; Finlay, M.R.; Fuentes Solis, N.O.; Hofman, G.L.; Jarousse, C; Koonen, E.; Keiser, D.; Lemoine, P.; Leenaers, A.; Marshall, F.; Meyer, M.; Muhammed Nor, A.W.; Park, Jong-Man; Ryu, Ho Jin; Shropshire, K; Snelgrove, J.; Swainson, I.; Van den Berge, S.; Wachs, D.; Wang, N.;, "Material Properties of Unirradiated Uranium-Molybdenum (U-Mo) Fuel for Research Reactors," International Atomic Energy Agency, 2020, vol. 1923.

[16] Y. S. Kim, G. L. Hofman, A. M. Yacout, and T. K. Kim, "U–Mo alloy fuel for TRU-burning advanced fast reactors," *J Nucl Mater,* vol. 441, no. 1, pp. 520-524, 2013/10/01/ 2013, doi: https://doi.org/10.1016/j.jnucmat.2013.01.324.

[17] Y. S. Kim and G. L. Hofman, "Fission product induced swelling of U–Mo alloy fuel," *J Nucl Mater,* vol. 419, no. 1-3, pp. 291-301, 2011, doi: 10.1016/j.jnucmat.2011.08.018.

[18] M. J. Mehl, D. Hicks, C. Toher, O. Levy, R. M. Hanson, G. Hart, and S. Curtarolo, "The AFLOW Library of Crystallographic Prototypes: Part 1," *Computational Materials Science,* vol. 136, pp. S1-S828, 2017/08/01/ 2017, doi: https://doi.org/10.1016/j.commatsci.2017.01.017.

[19] Y. S. Kim, G. L. Hofman, S. L. Hayes, and Y. H. Sohn, "Constituent redistribution in U-Pu-Zr fuel during irradiation," *J Nucl Mater,* vol. 327, no. 1, pp. 27-36, 2004/04/01/ 2004, doi: https://doi.org/10.1016/j.jnucmat.2004.01.012.

[20] F. R. W. Group, "Nuclear Metal Fuel: Characteristics, Design, Manufcaturing, Testing and Operating History," Nuclear Regulatory Commission, June 2018, issue 18-01.

[21] A. Wright, S. L. Hayes, T. H. Bauer, H. Chichester, G. Hofman, J. R. Kennedy, T. K. Kim, Y. S. Kim, R. Mariani, W. Pointer, A. Yacout, and d. Yun, "Development of advanced ultra-high burnup SFR metallic fuel concept - Project overview," *Transactions of the American Nuclear Society,* vol. 106, pp. 1102-1105, 01/01 2012.

[22] W. Zhuo, Y. Xie, M. T. Benson, H. Wu, R. D. Mariani, and J. Zhang, "Experimental assessment of antimony (Sb) in pure uranium for immobilizing fission product lanthanides," *J Nucl Mater,* vol. 534, p. 152135, 2020/06/01/ 2020, doi: https://doi.org/10.1016/j.jnucmat.2020.152135.

[23] Y. Xie and M. T. Benson, "Microstructure and diffusion behavior of uranium fuel with minor additives," *J Nucl Mater,* vol. 535, p. 152200, 2020/07/01/ 2020, doi: https://doi.org/10.1016/j.jnucmat.2020.152200.

[24] R. Khanal, N. Jerred, M. T. Benson, Y. Xie, R. D. Mariani, I. Charit, and S. Choudhury, "Interactions and immobilization of lanthanides with dopants in uranium-based metallic fuels," *J Nucl Mater,* vol. 540, p. 152372, 2020/11/01/ 2020, doi: https://doi.org/10.1016/j.jnucmat.2020.152372.

[25] R. Khanal, N. Jerred, M. T. Benson, D. A. Andersson, R. D. Mariani, I. Charit, and S. Choudhury, "A novel approach to selection of dopant to immobilize neodymium in uranium-based metallic fuels," *J Nucl Mater,* vol. 529, p. 151922, 2020/02/01/ 2020, doi: https://doi.org/10.1016/j.jnucmat.2019.151922.

[26] N. D. Jerred, R. Khanal, M. T. Benson, E. Perez, J. A. King, M. Dubey, J. Burns, I. Charit, S. Choudhury, and R. D. Mariani, "Evaluation of Tellurium as a Fuel Additive in Neodymium-Containing U-Zr Metallic Fuel," *Scientific Reports,* vol. 9, no. 1, p. 16043, 2019/11/05 2019, doi: 10.1038/s41598-019-51852-z.

[27] Y. Xie, J. Zhang, M. T. Benson, and R. D. Mariani, "Diffusion behavior of lanthanide-additive compounds (Ce4Sb3, Ce2Sb, and CeTe) against HT9 and Fe," *Materials Characterization,* vol. 150, pp. 107-117, 2019/04/01/ 2019, doi: https://doi.org/10.1016/j.matchar.2019.02.012.

[28] Y. Xie, J. Zhang, M. T. Benson, J. A. King, and R. D. Mariani, "Assessment of Te as a U-Zr fuel additive to mitigate fuel-cladding chemical interactions," *J Nucl Mater,* vol. 513, pp. 175-184, 2019/01/01/ 2019, doi: https://doi.org/10.1016/j.jnucmat.2018.10.050.

[29] R. D. Mariani, D. L. Porter, T. P. O'Holleran, S. L. Hayes, and J. R. Kennedy, "Lanthanides in metallic nuclear fuels: Their behavior and methods for their control," *J Nucl Mater,* vol. 419, no. 1, pp. 263-271, 2011/12/01/ 2011, doi: https://doi.org/10.1016/j.jnucmat.2011.08.036.

[30] C. M. Hin, Dane; Yu, Jianguo; Papesh, Cynthia, "Thermal Conductivity of Metallic Fuel," in "NEUP Final Project Report," Virginia Tech, 14-6767.

[31] J.-i. T. Nakamura, Yoichi; Izumi, Shin-ichiro; Kanno, Masayoshi, "Heat Capacity of Metallic Uranium and Thorium from 80 to 1000K," *J Nucl Mater,* vol. 88, p. 9, 1980.

[32] H. Jang, J. Louis-Jean, B. Childs, K. Holliday, D. Reilly, M. Athon, K. Czerwinski, D. Hatchett, and F. Poineau, "Synthetic diversity in the preparation of metallic uranium," *Royal Society Open Science,* vol. 9, no. 3, p. 211870, 2022/03/23 2022, doi: 10.1098/rsos.211870.

[33] D. H. Janney, Steven, "Experimentally known properties of U-10Zr alloys: A critical review," INL, 2018.

[34] J. L. S. Bates, J.B.; Bergenlid, U; Hochel, J.; Holzer, R.; Jakes, D: Leblanc, J.M.; Lyons, M.F.; Moretti, S.; Nishijima, T; Notley, M.J.; Stora, J.P.; Holley, C., "Thermal Conductivity of Uranium Dioxide," 1966.

[35] B. M. Ma, *Nuclear reactor materials and applications / Benjamin M. Ma* (no. Accessed from https://nla.gov.au/nla.cat-vn1731996). New York: Van Nostrand Reinhold Co, 1983.

[36] B. Szpunar and J. A. Szpunar, "Thermal Conductivity of Uranium Nitride and Carbide," *International Journal of Nuclear Energy,* vol. 2014, p. 178360, 2014/09/01 2014, doi: 10.1155/2014/178360.

[37] Y. Takahashi, M. Murabayashi, Y. Akimoto, and T. Mukaibo, "Uranium mononitride: Heat capacity and thermal conductivity from 298 to 1000 °K," *J Nucl Mater,* vol. 38, no. 3, pp. 303-308, 1971/03/01/ 1971, doi: https://doi.org/10.1016/0022-3115(71)90059-6.

[38] G. Vasudevamurthy and A. T. Nelson, "Uranium carbide properties for advanced fuel modeling – A review," *J Nucl Mater,* vol. 558, p. 153145, 2022/01/01/ 2022, doi: https://doi.org/10.1016/j.jnucmat.2021.153145.

[39] B. E. Alliance. "Advanced Test Reactor." https://inl.gov/atr/ (accessed 01/16/23, 2023).

[40] M. A. W. J. L. Williamson, "Pyroprocessing Flowsheets for Recycling Used Nuclear Fel," *Nuclear Engineering and Technology,* vol. 43, no. No. 4, p. 6, July 28, 2011 2011.

[41] M. A. Chen, Y. F. Xiong, W. Y. Jing, J. P. Jia, and P. C. Zhang, "Characterization of gamma-U-10 wt.%Mo alloy powders obtained by hydride-milling-dehydride

process," (in English), *J Nucl Mater,* vol. 400, no. 1, pp. 69-72, May 1 2010, doi: 10.1016/j.jnucmat.2010.02.011.

[42] M. Durazzo, C. J. da Rocha, J. Mestnik, and R. M. L. Neto, "Fabrication of Powder from Ductile U-Mo Alloys for Use as Nuclear Dispersion," (in English), *Mater Sci Forum,* vol. 727-728, pp. 362-367, 2012, doi: 10.4028/www.scientific.net/MSF.727-728.362.

[43] X. O. Yi-Fu, C. Miao, J. Wen-Yong, and C. Chang-An, "Manufacturing of U-10 wt% Mo powder by hydride-dehydride processing," (in English), *Fusion Eng Des,* vol. 85, no. 7-9, pp. 1492-1495, Dec 2010, doi: 10.1016/j.fusengdes.2010.04.012.

[44] M. K. Meyer, J. Gan, J. F. Jue, D. D. Keiser, E. Perez, A. Robinson, D. M. Wachs, N. Woolstenhulme, G. L. Hofman, and Y. S. Kim, "IRRADIATION PERFORMANCE OF U-Mo MONOLITHIC FUEL," *Nuclear Engineering and Technology,* vol. 46, no. 2, pp. 169-182, 2014, doi: 10.5516/net.07.2014.706.

[45] F. B. D. Vaz de Oliveira, M; Urano de Carvalho, E.F.; Saliba-Silva, A.M., "Powder Formation of Gamma Uranium-Molybdenum Alloys via Hydration-Dehydration," presented at the RERTR-2007 International Meeting on Reduced Enrichment for Research and Test Reactors, Prague, September 23-27, 2007, 2007.

[46] M. A. Steiner, C. A. Calhoun, R. W. Klein, K. An, E. Garlea, and S. R. Agnew, "alpha-Phase transformation kinetics of U-8 wt% Mo established by in situ neutron diffraction," (in English), *J Nucl Mater,* vol. 477, pp. 149-156, Aug 15 2016, doi: 10.1016/j.jnucmat.2016.05.016.

[47] S. Pasebani, "Processing of Oxide Dispersion Strengthened Alloys via Mechanical Alloying and Spark Plasma Sintering," Dissertation, Materials Science and Engineering, University of Idaho, 2014.

[48] B. S. Murty, J. Joardar, and S. K. Pabi, "Influence of Fe and Cr on the disordering behavior of mechanically alloyed NiAl," *Nanostructured Materials,* vol. 7, no. 6, pp. 691-697, 1996/08/01/ 1996, doi: https://doi.org/10.1016/0965-9773(96)00032-3.

[49] K. H. S. Singh, "Production of nanocrystalline nickel aluminides by mechanical alloying.," Indian Institute of Technology, Indian Institute of Technology, 1995.

[50] E. S. Park, D. T. Hoelzer, and R. A. Condrate, "Analysis of the interface between plasma-sprayed calcium phosphate coating and Ti-6Al-4V," (in English), *Mat Res S C,* vol. 458, pp. 409-414, 1997. [Online]. Available: https://www.webofscience.com/wos/woscc/full-record/WOS:A1997BJ28D00061?SID=USW2EC0D5BOWoIGYbyadtJ2zBwL93.

[51] S. Chatain, C. Guéneau, D. Labroche, O. Dugne, and J. Rogez, "Thermodynamic assessment of the Fe-U binary system," *Journal of Phase Equilibria,* vol. 24, no. 2, pp. 122-131, 2003/04/01 2003, doi: 10.1361/105497103770330730.

CHAPTER 3
Synthesis of U-10Mo Powder

3.1 Introduction

Since the 1960's, uranium-molybdenum (U-Mo) fuels have been examined for use in fast reactors and research reactors. The typical form for this fuel was in rolled plates, cast rods, and discs [1]. Since the late 1990s, new efforts in creating metallic nuclear fuels have utilized a powder metallurgy approach in order to create a dispersion fuel in rolled plates. Headed by the Reduced Enrichment for Research and Test Reactors (RERTR) initiative, methods to create a stabilized base centered cubic (BCC, also called γ-phase) U-Mo powder were developed through centrifugal atomization and hydride dehydride techniques [2-6].

U-Mo powder would be rolled between sheets of aluminum cladding that could then be implemented into research reactors needing to operate at lower temperatures, but with a higher content of uranium in the fuel compared to traditional UO_2.

For this work, U-10Mo (10 wt% molybdenum) powder was needed as a feedstock for mechanical alloying and spark plasma sintering experiments that are expounded on in Chapter 4.

A primary method of creating metallic fuel powder at the Idaho National Laboratory, and across the RERTR initiative, is through centrifugal atomization. Unlike gas atomization, the rotating electrode process (REP) utilizes a tungsten anode and the U-Mo cast rodlet as the consumable cathode as seen in Figure 3.2. The fuel is rotated on a spindle (typically on the order of tens of thousands of rpm), and the tungsten electrode strikes an arc, rapidly melting the fuel. Droplets of the U-Mo are flung off radially, and cool while in flight, before striking a powder catch basin. This activity is performed in an argon atmosphere (<50 ppm O_2) to prevent alloy contamination that would ensue by atomizing in a nitrogen or air atmosphere [1, 2, 7, 8]. While a beneficial and reliable method, the REP's drawbacks include low powder yield (40-50% mass loss due to unusable material like sprue held inside the chuck and process loss) and large particle size (~100-300 μm for U-Mo).

An additional approach was briefly investigated for creating U-10Mo powder, which was a hydride-dehydride (HDH) method to breaking up U-Mo rodlets. The HDH powder

production method was noted in the past for being successful in creating U-Mo alloy powder [5, 6]. The HDH method has been utilized in creating metallic uranium powder since the 1950's. The premise of this process being that uranium hydride has a lower density than that of uranium metal, in addition to a drastic difference in lattice constant, causing it to flake off of a uranium ingot when introduced to hydrogen [9, 10]. Once all available uranium sites have been hydrided, as indicated by hydrogen flow rate decreasing to zero within the chamber, the reactor chamber is heated up to release the hydrogen, yielding metallic uranium once more. This process is repeated until a fine U powder (~38 μm) is created. The chemical reaction is thus shown.

$$2U + 3H_2 \leftrightharpoons 2UH_3$$

3.2 Materials and Methods

3.2.1 Initial Alloying of U-10Mo

Before researching the feasibility of creating UN nanoparticles within U-Mo alloys, a U-10Mo powder had to be created itself. This was done by alloying depleted uranium and molybdenum in the correct weight ratios, arc-casting the alloy buttons into rodlets, then powderising said rodlets using a custom in-house atomizer.

Feedstock U-10Mo production was achieved by arc melting molybdenum foil and depleted uranium pieces in a water-cooled copper hearth and tungsten electrode setup (Figure 3.1). Alfa Aesar 99.95% pure Mo foil was used for the 10 wt% addition in the alloy, and EBR II depleted uranium axial blanket pins were used for the uranium addition.

Figure 3.1: Single probe arc melting setup (above) and arc melted button to cast U-10Mo pin transition (below) in preparation for atomization. Partial pressure of O_2 inside the glovebox always kept below 50 ppm for casting activities, and typical O_2 levels were below 10 ppm. Partial pressure of N_2 is not recorded within this glovebox.

These arc melted pins needed powderising, so both a novel hydride-dehydride and centrifugal atomization technique were attempted.

3.2.2 Centrifugal Atomization Technique

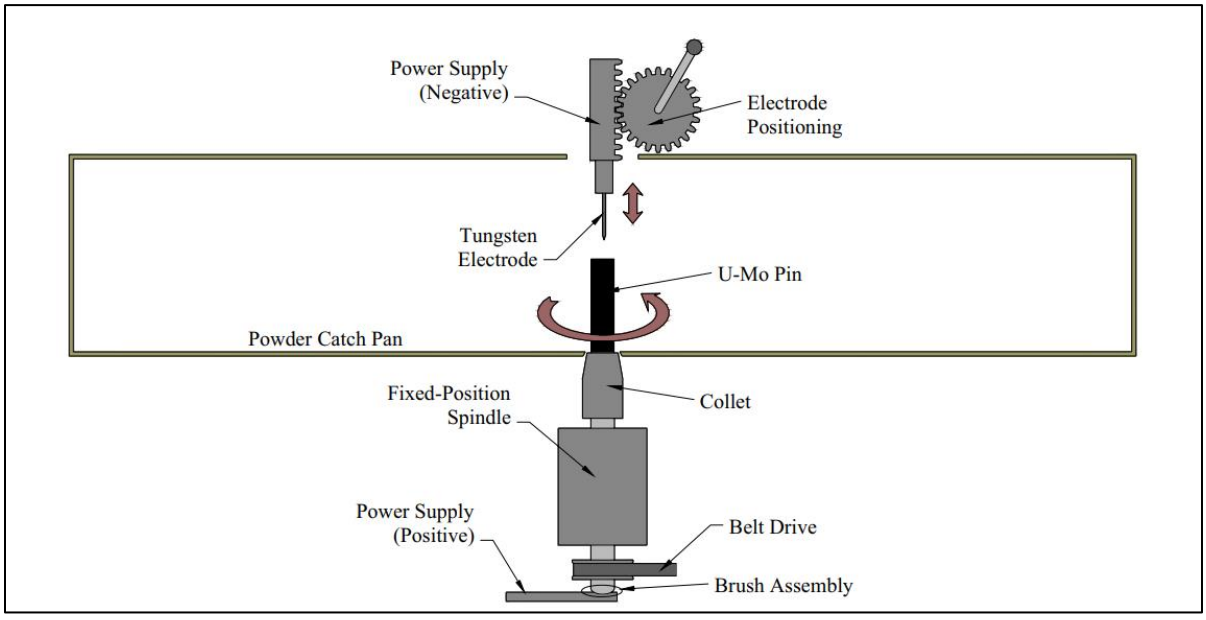

Figure 3.2: Schematic of the Idaho National Laboratory's legacy centrifugal atomizer. Through the rotating electrode process, molten droplets of U-Mo fuel would be dispersed radially, and cool before striking the powder catch pan, producing pseudo-spherical powder [7].

The primary method utilized for U-10Mo powder production was atomization. Cast rodlets were loaded into a custom-built lab-scale atomizer where they were rapidly spun while an arc was struck on the surface of the sample. Droplets of molten U-10Mo were distributed radially away from the rodlet and cooled to a solid state while in flight before being collected in the catch pan. All atomization took place within an inert argon atmosphere with an oxygen content <50 ppm O_2. Nitrogen and water content within the glovebox was not measured for this research.

3.2.3 Hydride-Dehydride Powder Production Technique

A novel hydride-dehydride method of forming U-10Mo powder was pursued as well. Arc melted pins of γ-phase U-10Mo were heat treated at 570 ℃ for 24 hours to induce an α-phase uranium formation that would more readily form powder during the HDH cycling. This heat-treated pin was then placed into a Thermo Scientific Lindberg Blue tube furnace and cycled in hot hydrogen five times at 275 ˚C before a final burn off of the hydrogen. This temperature was utilized for hydrogen cycling, as it has experimentally shown to be the most favorable temperature for hydride-dehydride reactions of metallic uranium with the setup at FASB.

In a second attempt, the previous operating temperature for heat treatment was thought to be too high for forming α-phase based on the time-temperature-transition (TTT) diagram referenced by Jana et al [11]. Pieces of U-10Mo cast rod were heat-treated at 500 ℃ for 30 hours to induce the partial α-phase. These heat-treated castings were hydrogen cycled five times in a custom-built furnace at the Experimental Fuels Facility (EFF). Both attempts resulted in non-reportable amounts of powder being produced. No further efforts were made to create U-10Mo powder this way due to the ease in which the lab-scale atomizer could produce the desired product, and the pertinent work needing moved on to keep on schedule.

3.2.4 Analysis

A JSM-IT500 HR SEM, Oxford Instruments Ultimax 65 EDS, and Malvern-Panalytical Aeris XRD (Cu-kα source) were utilized to obtain the results for arc-melted U-10Mo, heat-treated ingots, and atomized powder. XRD powder samples were encapsulated in vacuum grease to prevent oxidation outside of the glovebox, and cross sections were cut from the cast and heat-treated U-10Mo ingots for use as SEM and XRD samples. These cross sections

along with atomized powder that was suspended in epoxy were polished to a 1 μm surface finish before SEM analysis.

3.3 Results and Discussion

XRD plots and SEM micrographs of the feedstock uranium as well as the U-10Mo cast rods (both heat-treated and non-heat treated) and atomized powder were gathered. Feedstock uranium from the EBR-II blanket pins was found to be an orthorhombic α-phase as shown by the XRD plot in Figure 3.3A. Both the heat-treated (570 ℃ for 24 hours) and non-heat-treated U-10Mo cast pins showed γ-phase retention after arc melting (Figure 3.3B and 3.3C), but no alpha phase formation was noted in the heat-treated material. International Center for Diffract Data (ICDD) reference numbers utilized in this work for α-U and γ-U-10Mo phases are 00-011-0628 and 00-054-0497 respectively.

While no alpha phase was noted via XRD analysis, when examining the heat-treated vs. the non- using SEM and energy dispersive X-Ray spectroscopy (EDS) there was evidence of a uranium rich phase forming at the grain boundaries of the γ-U-10Mo. This is outlined in Figure 3. Both uranium rich and uranium poor zones are typical in the U-Mo BCC system, and the EDS maps and linescans revealed exacerbation of this behavior after heat treatment for 24-hours.

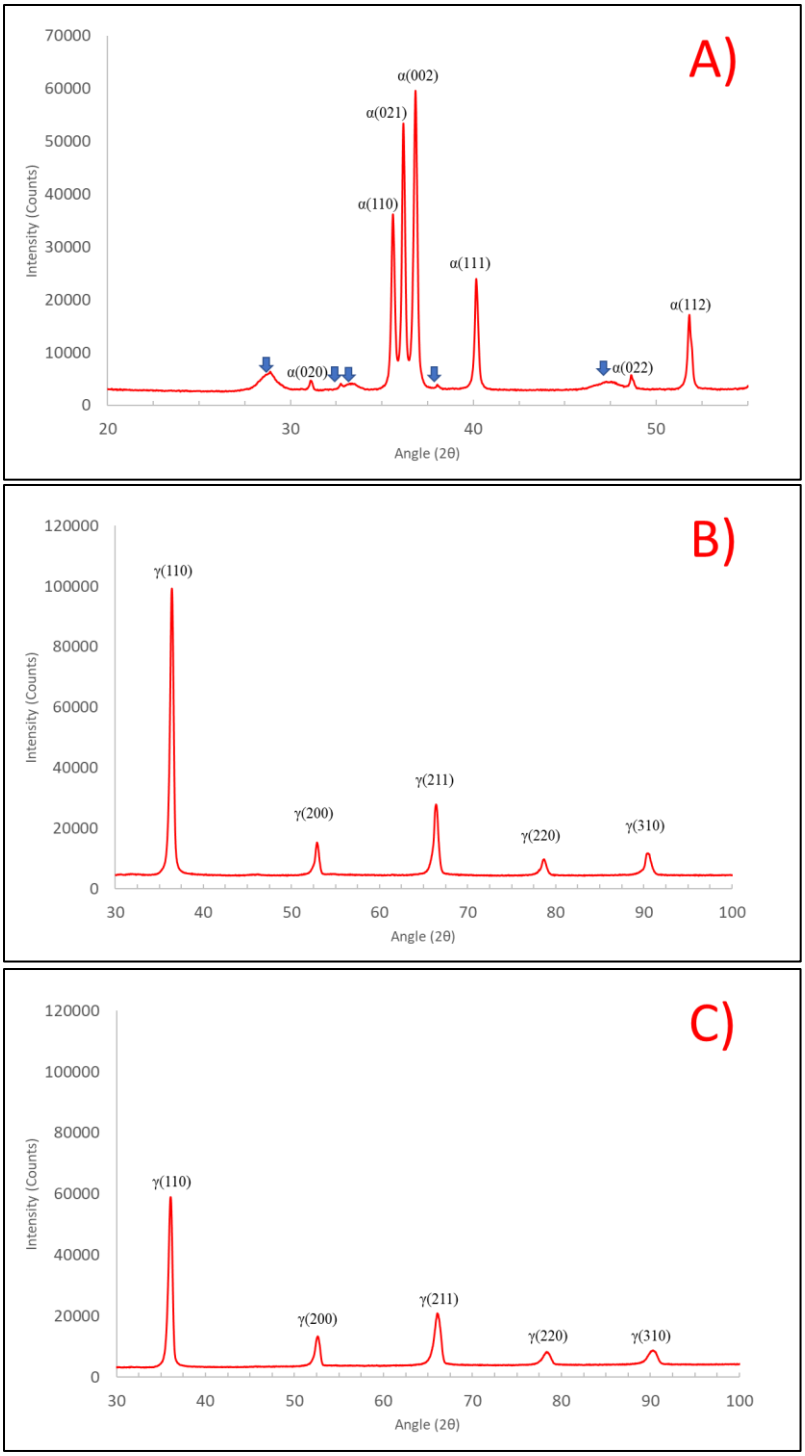

Figure 3.3: XRD peaks taken of depleted U-feedstock (A) Arc melted U-10 Mo (B) and heat-treated U-10Mo cast rod for 24 hours at 570 °C (C). Alpha phase orthorhombic peaks are indexed for the feedstock uranium. The other peaks marked with blue arrows are varying U_xO_y peaks, presumably due to oxidation. No peak change was seen from stock U-10Mo and the heat-treated U-10Mo other than reduced peak intensity after the 24-hour heat treatment.

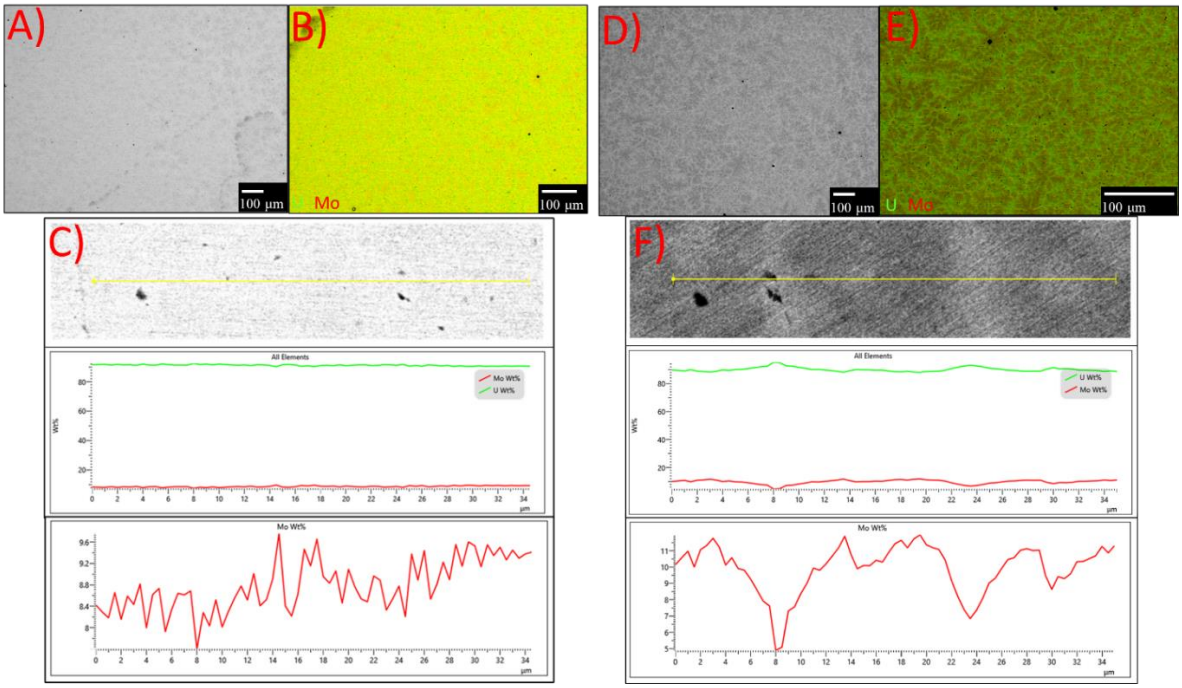

Figure 3.4: Backscatter electron micrograph, EDS map and line scan of "as-cast" U-10Mo (A, B, and C) and 24 h 570 °C heat-treated (D, E, and F). Segregation of the uranium and molybdenum from solid solution are beginning to be seen in the map and line scan shown in E and F

In order to obtain results in a reasonable time, atomization was a proven method, and was pursued for remaining feedstock powder production despite the process loss incorporated with that method. Atomized powder analyzed in the SEM showed a mixed morphology, with only a small amount of the resultant material being spherical, and most being ellipsoid or angular in shape. Compositionally, the uranium and molybdenum content was dispersed homogenously across the powder particles. The powder cross sections were tallied manually across thirty specimens, and average particle size was found to be 190 µm, with powders varying in size from 100-300 µm (Figure 3.5).

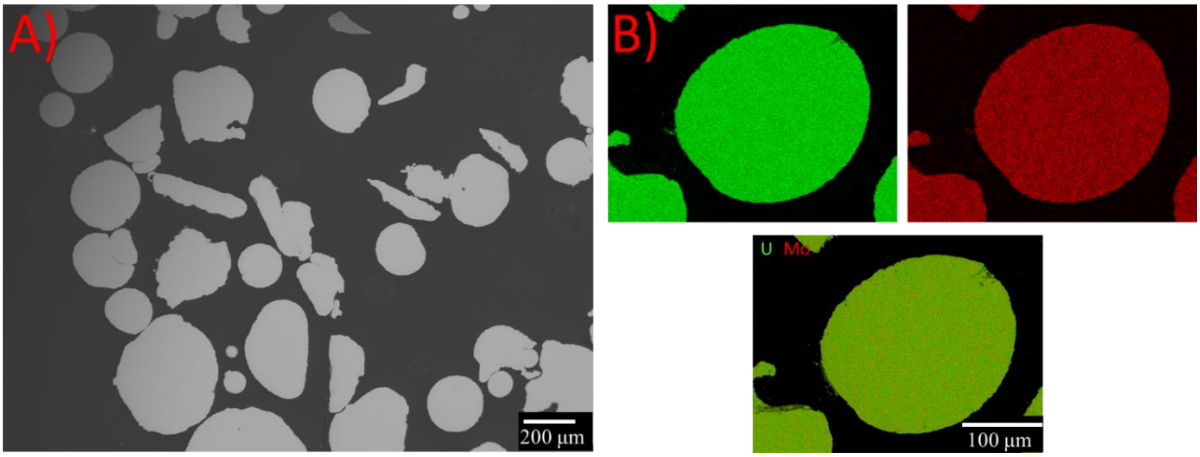

Figure 3.5: (A) SEM micrograph depicting the average particle size and shape of atomized U-10Mo. Differences in geometry hypothesized to be due to some molten U-Mo particles cooling and spheroidizing in argon, while others striking the wall of the atomizer catch basin while still molten, forming longer plate-like geometries when recovered. (B) Separate EDS maps showing the uranium (green) and molybdenum (red) distribution across a fuel cross section. Homogeneity of the uranium and molybdenum was noted across the entire powder sampling.

3.4 Conclusions

A stabilized γ-phase U-10Mo powder feedstock was needed before research in implantation of UN into a metallic fuel matrix could begin. This work successfully created said feedstock by alloying via arc-melter and atomizing of the cast pins into a powder. The atomized powder particles had an average diameter of 190 µm, containing both angular and spherical geometries. Uranium and molybdenum content was homogenous across the feedstock powder, and γ-phase was confirmed via XRD analysis.

Due to substantial process loss of material during atomizing via unusable sprue, a second method of powderising the U-10Mo castings was pursued through a novel hydride-dehydride method. The cast U-10Mo pins were heat treated at both 570 ℃ for 24 hours and 500 for 30 hours to induce a partial α-phase. These heat-treated castings were then hydrogen-cycled five times. Upon removal from the HDH furnace, neither sample achieved substantial breakup into a powder form. It is hypothesized that not enough alpha phase could form with 10 wt% Mo present in the system, since it acted as a stabilizer for the γ-phase.

3.5 References

[1] J. Horak, J. Reuscher, and D. Sasmor, "Operating experience with uranium--molybdenum fuel in pulsed reactors," Sandia Labs, Albuquerque, N. Mex.(USA), 1973.

[2] K. H. Kim, D. B. Lee, C. K. Kim, G. E. Hofman, and K. W. Paik, "Characterization of U-2 wt% Mo and U-10 wt% Mo alloy powders prepared by centrifugal atomization," *J Nucl Mater,* vol. 245, no. 2, pp. 179-184, 1997/06/01/ 1997, doi: https://doi.org/10.1016/S0022-3115(97)00011-1.

[3] B. P. Balart S., Granovsky M., Gribaudo L., Hermida J., Ovejero J., Rubiolo G., Vincente E., "U-Mo Alloy Powder Obtained by a Hydride-Dehydride Process," presented at the International Meeting on Reduced Enrichment for Research and Test Reactors, Las Vegas, Nevada, 2000, Conference Paper.

[4] X. O. Yi-Fu, C. Miao, J. Wen-Yong, and C. Chang-An, "Manufacturing of U-10 wt% Mo powder by hydride-dehydride processing," (in English), *Fusion Eng Des,* vol. 85, no. 7-9, pp. 1492-1495, Dec 2010, doi: 10.1016/j.fusengdes.2010.04.012.

[5] M. Durazzo, C. J. da Rocha, J. Mestnik, and R. M. L. Neto, "Fabrication of Powder from Ductile U-Mo Alloys for Use as Nuclear Dispersion," (in English), *Mater Sci Forum,* vol. 727-728, pp. 362-367, 2012, doi: 10.4028/www.scientific.net/MSF.727-728.362.

[6] M. A. Chen, Y. F. Xiong, W. Y. Jing, J. P. Jia, and P. C. Zhang, "Characterization of gamma-U-10 wt.%Mo alloy powders obtained by hydride-milling-dehydride process," (in English), *J Nucl Mater,* vol. 400, no. 1, pp. 69-72, May 1 2010, doi: 10.1016/j.jnucmat.2010.02.011.

[7] C. R. Clark, B. R. Muntifering, and J. F. Jue, "Production and Characterization of Atomized U-Mo Powder by the Rotating Electrode Process," presented at the The RERTR-2007 International Meeting on Reduced Enrichment for Research and Test Reactors, Prague, Czech Republic, September 23, 2007, 2007.

[8] K.-H. Kim, D.-B. Lee, C.-K. Kim, I. H. Kuk, and G. L. Hofman, "Development of high-loading U-Mo alloy fuel by centrifugal atomization," IAEA, 1996-10-01 1996, Argonne National Laboratory, 9700 S. Cass Avenue, Argonne, IL 60439 (United States). [Online]. Available: https://www.osti.gov/etdeweb/servlets/purl/20521089. [Online]. Available: https://www.osti.gov/etdeweb/servlets/purl/20521089

[9] A. Banos, N. J. Harker, and T. B. Scott, "A review of uranium corrosion by hydrogen and the formation of uranium hydride," *Corrosion Science,* vol. 136, pp. 129-147, 2018/05/15/ 2018, doi: https://doi.org/10.1016/j.corsci.2018.03.002.

[10] M. K. Clark C.R.; Meyer, "Fuel Powder Production from Ductile Uranium Alloys," Argonne National Laboratory, October 18, 1998 1998.

[11] S. Jana, A. Devaraj, L. Kovarik, B. Arey, L. Sweet, T. Varga, C. Lavender, and V. Joshi, "Kinetics of cellular transformation and competing precipitation mechanisms during sub-eutectoid annealing of U10Mo alloys," *Journal of Alloys and Compounds*, vol. 723, pp. 757-771, 2017/11/05/ 2017, doi: https://doi.org/10.1016/j.jallcom.2017.06.292.

CHAPTER 4

UN Nanostructure Evolution in Mechanically Alloyed Powders and Spark-Plasma Sintered U-10Mo Fuels

4.1 Introduction

Mechanical alloying is a process in which a metal or alloy powder is placed into a milling jar along with a trace amount of oxide such as Y_2O_3 or Ce_2O_3, and a milling media. The jar is then sealed, and energy is deposited through rapid rotating motion, typically on the order of 200-1,700 rpm [1-3]. As the media collide during the milling process, the trace amounts of oxide are broken into smaller pieces and driven into the metallic matrix creating nanometric oxide structures spread homogenously in the powder feedstock. These nano-oxides provide a multitude of benefits to the metal alloy, including increased strength, corrosion resistance, and low swelling behavior in high dose ion-irradiation environments [4]. The low swelling during irradiation is theoretically due to fission products being trapped at vacancy sites within the nano-oxide due to the high sink strength present at the interface between the nano-oxide and the matrix material. Reported sink strength in ODS steel is reported in the range of $3.1 \times 10^{16}\ m^{-2}$ by Wu et al. [5].

In the past thirty years, the idea of mechanical alloying has been explored utilizing a gas overpressure during milling instead of adding an oxide. By pressurizing the jars with high purity nitrogen gas, TiN, ZrN, and Mo_2N have been successfully produced in other research [1, 6]. One difference between oxide and nitride mechanical alloying is that the utilization of a cover gas does not always form nanostructures. Often times the work conducted was meant to produce a bulk nitride phase, not a distributed nanophase. Ellingham diagrams of applicable oxide and nitride compounds compiled from past research [7-15] are compared below in Figure 4.1 to show stabilities of each nitride and oxide phase within a nitrogen gas system with oxygen contamination.

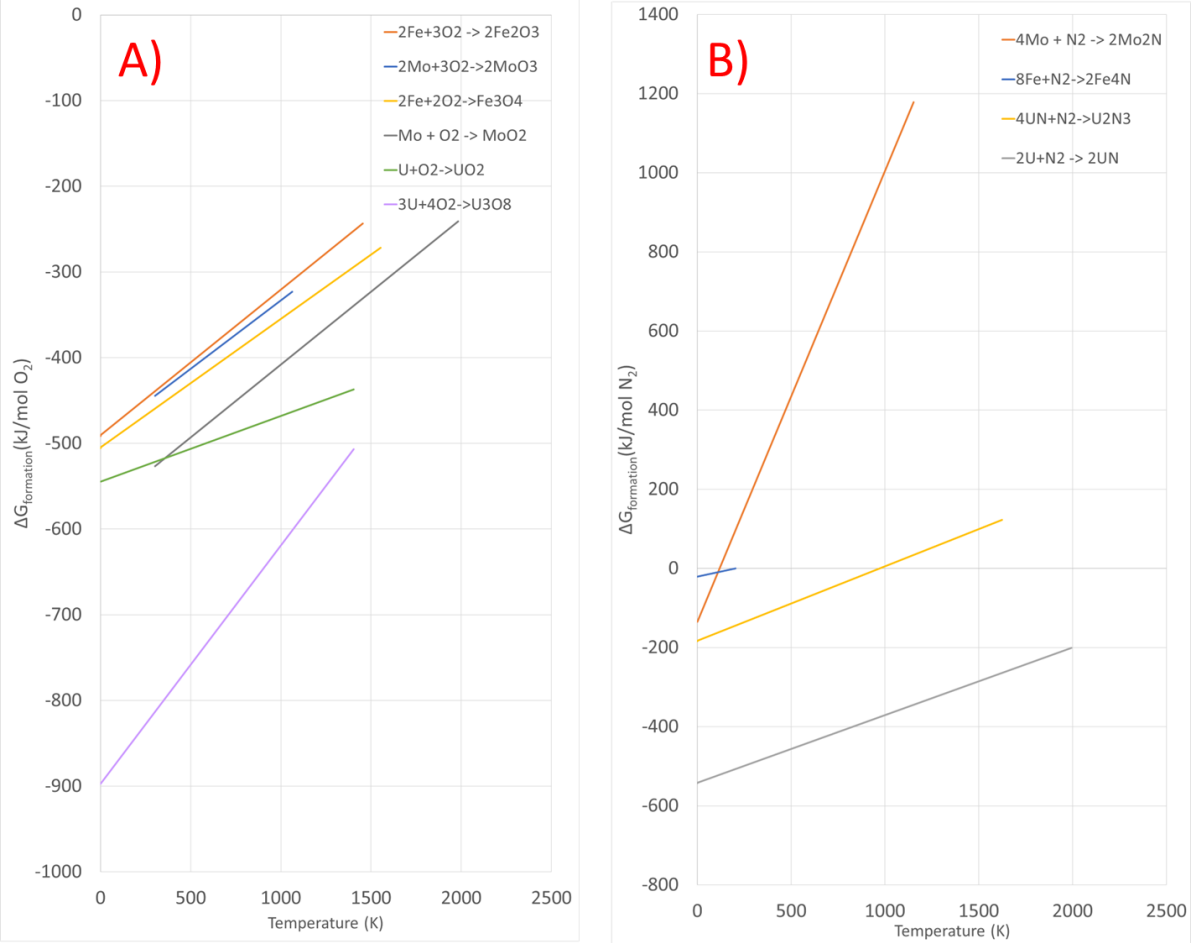

Figure 4.1: Compiled Ellingham diagrams for common oxides (A) and nitrides (B) for the iron, molybdenum, and uranium systems [7-15]. The data shows that UN and U_2N_3 develop more favorably than Fe_4N and Mo_2N under a N_2 atmosphere at temperature, but also that uranium oxides are even more likely to form within an O_2 atmosphere than their respective nitrides.

In this research, an effort to produce uranium mononitride nanoparticles within 90 wt% U/ 10 wt% Mo (U-10Mo) through a gaseous mechanical alloying process similar to that produced in previous studies was pursued.

Ideally, the milling process should homogenously distribute UN nanoparticles within the U-Mo matrix, producing a similar capability to uranium bearing metallic fuel that oxide nanoparticles produce for stainless steel. The posed benefit being the swelling reduction during irradiation that has been a major hinderance for utilization of U-Mo fuels in next generation nuclear reactors.

4.2 Materials and Methods

4.2.1 U-10Mo Mechanical Alloying Under N2 Atmosphere

Atomized U-10Mo feedstock powder was transferred to the Experimental Fuels Facility (EFF) at the Idaho National Laboratory – Materials and Fuels Complex (INL-MFC) for mechanical alloying. Using a 10:1 ball to powder weight ratio, 3 mm diam. stainless steel (SS) media and feedstock powder were loaded into a 50 mL Retsch stainless steel milling jar. From here, a Retsch aeration lid was clamped onto the top at 12.5 N-m torque, and high purity nitrogen (99.9995% pure) was introduced into the closed jar to a pressure of 40 psi. The jar setup was then loaded into a Retsch PM-200 and milled for 1, 10, 20, and 40 hours using this setup. This is visualized in Figure 4.2, showing the imbedding of nitrogen into the U-10Mo fuel powder through collision of the SS media during planetary milling.

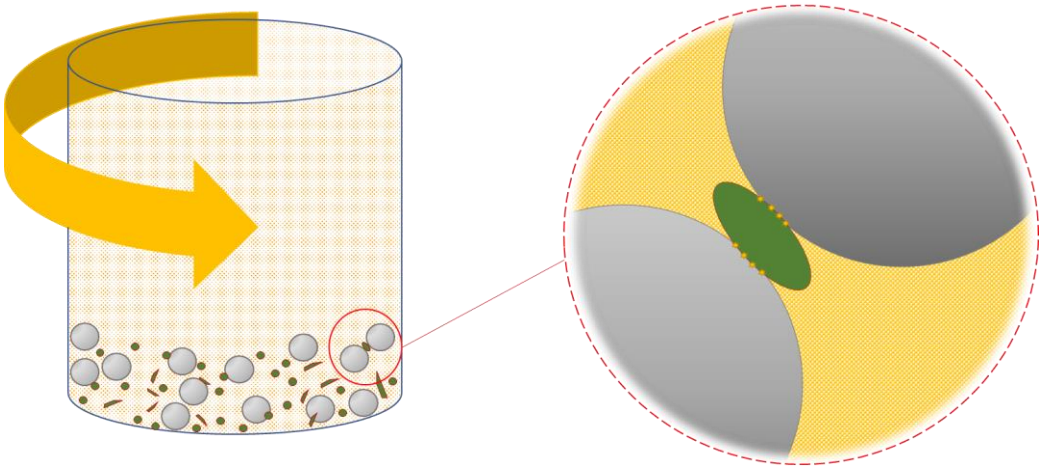

Figure 4.2: Milling jars were loaded with stainless steel media (grey spheres) and alloy powder (green particles), then are pressurized with a nitrogen cover gas (yellow gradient). Kinetic energy is inserted through centrifugal force and forces due to the Coriolis effect. When the milling media impact with the alloy powder

Another test was conducted to analyze the effects of milling media size on nitrogen uptake within the U-Mo system and was milled first with 3 mm media for 24 hours, then for 40 hours using 2 mm SS media. The point of utilizing 3 mm for 24 hours of the milling time was to see if reduction in milling media size would also reduce resultant U-10Mo powder size. After milling, the media and powder were separated using a sieve, and the milled powder was set aside for analysis. All powders were milled at 400 rpm with a 30 second cool-off time for every 1 minute of milling. The rpm was chosen based on the highest amount of energy that could be deposited while not imparting constructive interference between the milling jar and counterweight. Cool-off periods were implemented to prevent heat buildup

and potential damage to both the jar and U-10Mo powder. The 64-hour and 20-hour milled material was filled with nitrogen gas twice because of intermittent operations that had to take place before milling, such as changing of the media size, or removing a sample of milled powder. Milling parameters are tabulated in Table 4-1.

Table 4-1: Powder batch milling parameters.

Mill Time *(hours)*	**Aeration Count**	**Media Size *(mm)***
24/40 (64)	2	3/2
40	1	3
20	2	3
10	1	3
1	1	3

4.2.2 Heat-Treatment

A heat-treatment experiment was conducted on the 40-hour milled powder with a two-fold purpose. First being, to stabilize a UN phase in case nitrogen had simply been driven into interstitial spaces within the BCC lattice. The second purpose was to recrystallize the γ-phase U-10Mo for better resolution in XRD data, as extended milling of materials with stainless steel media has been reported to amorphize alloyed powder. For this experiment, a paper (Recrystallization kinetics of cold-rolled U-10 wt% Mo) by Frazier et. al. was referenced, and the powder was treated in an yttria crucible at 700 °C for 2 hours in a Thermo Scientific Lindberg Blue M tube furnace under argon atmosphere (<50 ppm O_2) to obtain a nearly fully recovered BCC structure [16]. The heat-treated powder was then analyzed in a PANalytical AERIS X-Ray Diffractometer (Cu-kα source).

4.2.3 Spark-Plasma Sintering

Three-gram batches of 1-hour and 40-hour milled U-10Mo powder were spark-plasma sintered (SPS) in a Thermal Technologies DCS-50 sintering furnace. The 40-hour milled U-10Mo was sintered at 900℃ and 40 MPa applied pressure for 20 minutes, while the 1-hour

milled material was sintered at 900℃ and 40 MPa for only 5 minutes. This change in dwell time was made to avoid melting by formation of a low-melting point U_6Fe phase that transpired in the 40-hour milled U-10Mo. was due to not wanting to risk melting by formation of a low-melting point. Similar low-melting points due to iron in a uranium system have been observed in previous research [17, 18]. Additionally, punch compression was not observed past five minutes into the hold, meaning that adequately high densities could be reached in a shorter hold-time at temperature.

4.2.4 Characterization

After milling and heat-treatment, several powder samplings and sintered compacts were analyzed via scanning electron microscope (SEM) on a JSM-IT500HR SEM, X-Ray Diffractometry (XRD) on a PANalytical Aeris XRD, light element analysis on an ELTRA ONH-2000, mass spectroscopy on “The Prodigy” inductively coupled plasma–atomic emission spectrometer (ICP-AES), scanning transmission electron microscopy (STEM) on a FEI Titan STEM, and atom probe tomography (APT) on the LEAP 5000 Atom Probe in order to quantify both the presence of nitrogen in the system, as well as quantify the number, size, and composition of nanostructured nitrides within the U-10Mo lattice material.

Powder samples from the 1, 10, and 40-hour milled U-10Mo as well as the 40-hour milled U-10Mo heat treated at 700 ℃ for 2 hours were transferred to the IMCL to create TEM lamellae using focused ion beam (FIB) techniques. Samples were taken from the surface of the powder particles and taken as deep as possible to best avoid the amorphous iron layer present in the outermost micrometers. The lamellae extraction process is visualized in Figure 4.3.

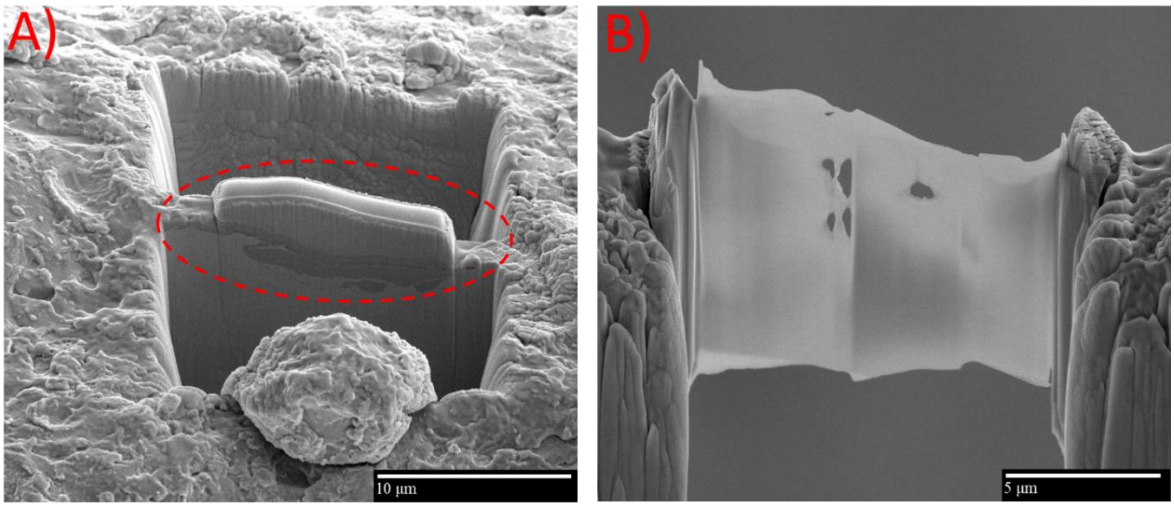

Figure 4.3: (A) 40-hour milled U-10Mo powder sample with TEM lamellae fabricated using FIB techniques. Circled in red show the top extended surface, which is the platinum deposit for sample manipulation, and lower grey streak is the revealed amorphous iron layer on powder surface. (B) TEM lamellae in grid mount in preparation for TEM analysis.

Lamellae from the four powder batches were then loaded onto a grid mount and then placed into a FEI Titan Scanning Transmission Electron Microscope (STEM) in IMCL for characterization.

XRD samples from the atomized, 1 hour, 10-hour, 20-hour, 40-hour milled, and 40-hour (with a 2-hour heat treatment at 700 ˚C) milled powder sets (3 mm media) were prepared by encapsulation within vacuum grease (to prevent exposure to air), then placed onto a zero-background holder, and were loaded into a PANalytical AERIS X-Ray Diffractometer (Cu-kα source).

4.3 Results and Discussion

4.3.1 Nitrogen Uptake in Milled U-10Mo

Samples from the 40-hour milled U-10Mo powder were sent for light-element analysis in the INL oxygen/nitrogen analyzer. Across five samples analyzed, nitrogen was found in 5700-9600 µg/g (ppm) quantities with an average of 7420 ppm. Due to the standard not being calibrated for that high of readouts, these numbers were deemed qualitative. Later on, 9 more samples were sent to be oxygen/nitrogen analyzed, calibrated at higher nitrogen readouts. Samplings were taken from three powder batches from the 1-,10-, and 40-hour (+ 700℃/2 hr.) milled U-10Mo. Figure 4.4 shows how the nitrogen and oxygen counts trended with increased milling time.

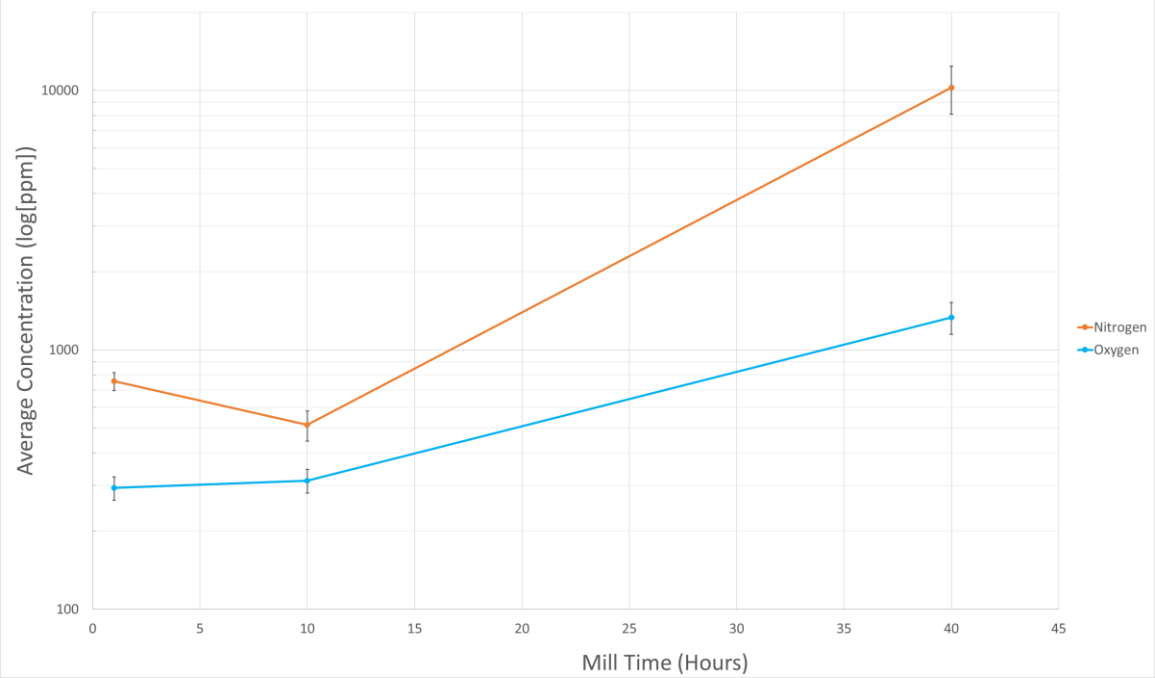

Figure 4.4: Light element analysis results for 1-10- and 40-hour milled + 700℃ /2 hr. heat treated material. An overall increase in nitrogen and oxygen content can be observed as a function of milling time. Data points and error bars are averaged across three separate samplings analyzed for each milled powder.

Results from the qualitative light element analysis seemed to align well with the quantitative results obtained on these three powder batch sets. The 10-hour milled material showed a decrease in nitrogen content, and a slight increase in oxygen content. It is not understood at the moment why this is, but after 10 hours, the nitrogen and oxygen content increased exponentially. Error bars were determined via the total propagated uncertainty from the scale measuring the mass of the material, signal error is bound up by the integration methods of the analyzer, and the error of the standard used. Uncertainty values were analyzed using GUM Workbench Pro Version 2.4.1.406. A derived relation between milling time and nitrogen gas uptake was not pursued as this experimental method was only used to answer if nitrogen had embedded itself into the alloy material prior to SEM, XRD, TEM, and APT analysis.

In the XRD data shown in Figure 4.5, substantial peak reduction was noted from the “as-cast” pin state to atomized powder, and again from atomized to the milled powder state. In literature this peak reduction is potentially due to iron contamination within the system, or amorphization during milling due to high dislocation density [19, 20]. Additionally, in the 10-hour, 20-hour, and 40-hour + heat treat milled powder XRD patterns, several characteristics were found that corresponded to UN, showing that even on a larger scale, UN

formation could be indexed within the powder after these mill-times. It is hypothesized that UN peaks were not seen in the 40-hour milled material because an amorphous iron layer had coated itself so much around the powder particulates that all other peaks were lost in the noise. For the 1-hour milled material, it is believed that not enough UN had formed to meaningfully diffract above background levels. International Center for Diffraction Data (ICDD) reference numbers for α-Fe, γ-U-10Mo and UN are 04-017-6071, 00-054-0497, and 04-003-5402 respectively.

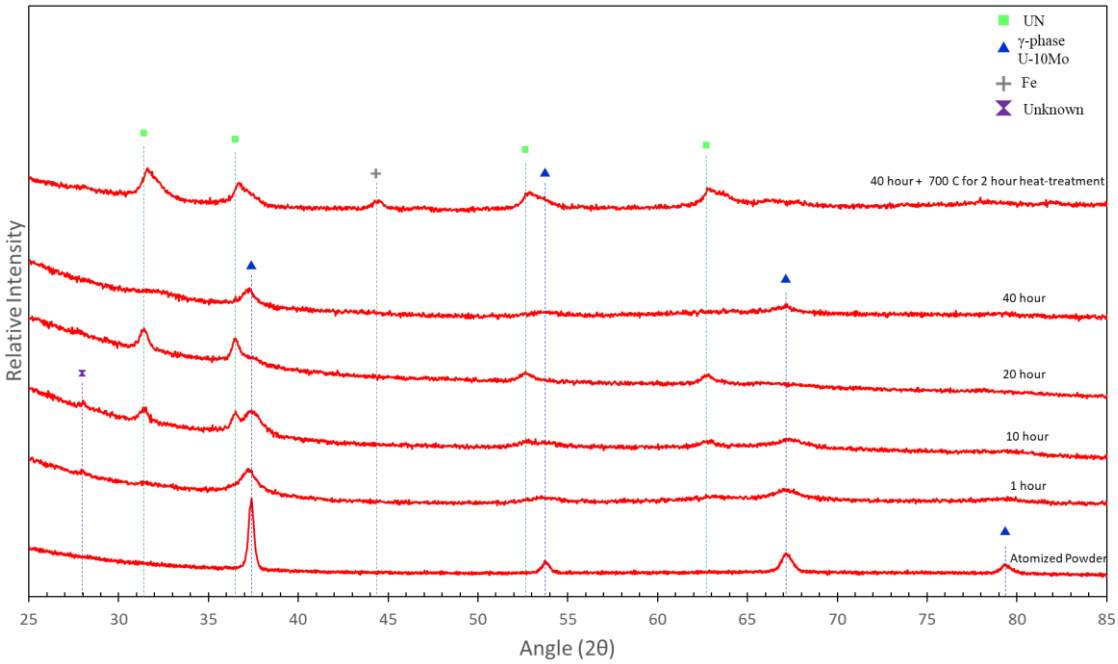

Figure 4.5: Stacked XRD patterns as a function of milling time in a nitrogen atmosphere. Peak intensity is reduced with increased milling time.

As is to be discussed further in section 4.3.4.5, UN nanoparticulates were found in abundance in both 1 and 40-hour milled material. The XRD patterns help show where the UN is forming, as, apart from the anomalous behavior in the non-heat treated 40-hour milled material, a peak transition occurs between 10-20 hours where a predominant UN BCC structure takes the place on the surface of the powders instead of the γ-phase U-10Mo. Since XRD operates on a near-surface range of depth between 1.5-3.5 μm, it aligns with other results showing the UN phase only forms at the surface boundaries of these powders and does not form homogenously across the volume of the alloyed powder (see Figures 4.13 and 4.15).

The 40-hour milled material was the first batch ran, meaning that neither the jar nor media had been used before the run. This may have caused additional iron contamination in the fuel that was not as pertinent in the 1,10-, and 20-hour tests, and would have blocked out any observable UN peaks through the amorphous noise.

The working theory of nitride formation within the U-10Mo lattice is as follows: As the mechanical alloying of the U-10Mo took place in N_2 gas, the alloy was heavily deformed through impacts with the stainless-steel media. This would have imparted little fracturing, due to the ductile nature of U-Mo, but still would result in substantial cold welding and material exchange between the alloy powder and media. On the atomistic scale, a great number of defects are driven through prolonged alloying [21], primarily seen in dislocation pile ups, increased grain boundaries, interstitial and substitutional defects, and loss of large-scale repeating order. With the high content of nitrogen present in the alloying environment, and an increased number of defect sites in the alloy, nitrogen is easily embedded into the fuel upon media impact (See Figure 4.2 for visualization). The formation of a nitride appears to happen instantaneously, as the nitrogen atoms are not in an energetically favorable state as interstitial defects. The triple bond between the two nitrogen atoms is hypothesized to be overcome by both the intense kinetic energy imparted during planetary milling, as well as the favorable formation energies of the UN and U_2N_3 molecules. With regard to which atoms nitrogen would preferentially compound with, the uranium nitride system has the most favorable outlook, with lower formation energies than both the Fe-N and Mo-N systems. These values are compared in Table 4-2, following that the more negative a formation energy is, the more stable the phase will be.

Table 4-2: Formation energies of uranium, molybdenum, and iron nitrides at 0 K [22, 23]

Binary Compound	Formation Energy (eV/atom)
UN	-1.416
U_2N_3	-1.513
UN_2	-1.495
Mo_2N	-0.309
MoN	-0.471
Mo_2N_3	-0.302
FeN	-0.229
Fe_3N	-0.127
Fe_8N	-0.055

The reason uranium mononitride forms in this system as opposed to the more energetically favorable U_2N_3 or UN_2 compounds is theoretically due to the lower partial pressure of nitrogen utilized while milling. It is reasonable to extrapolate that if a continuously aerating nitrogen system was utilized, a U_2N_3 or UN_2 phase would be formed instead [24]. Another variable that could affect UN stability would be temperature, as can be noted in the U-N phase diagram developed by Okamato et al [25] in Figure 4.6. It may be postulated that with increased temperatures for prolonged periods, the more stable uranium nitride phases may form upon cooldown, or perhaps cause agglomeration of nanoparticles into larger structures.

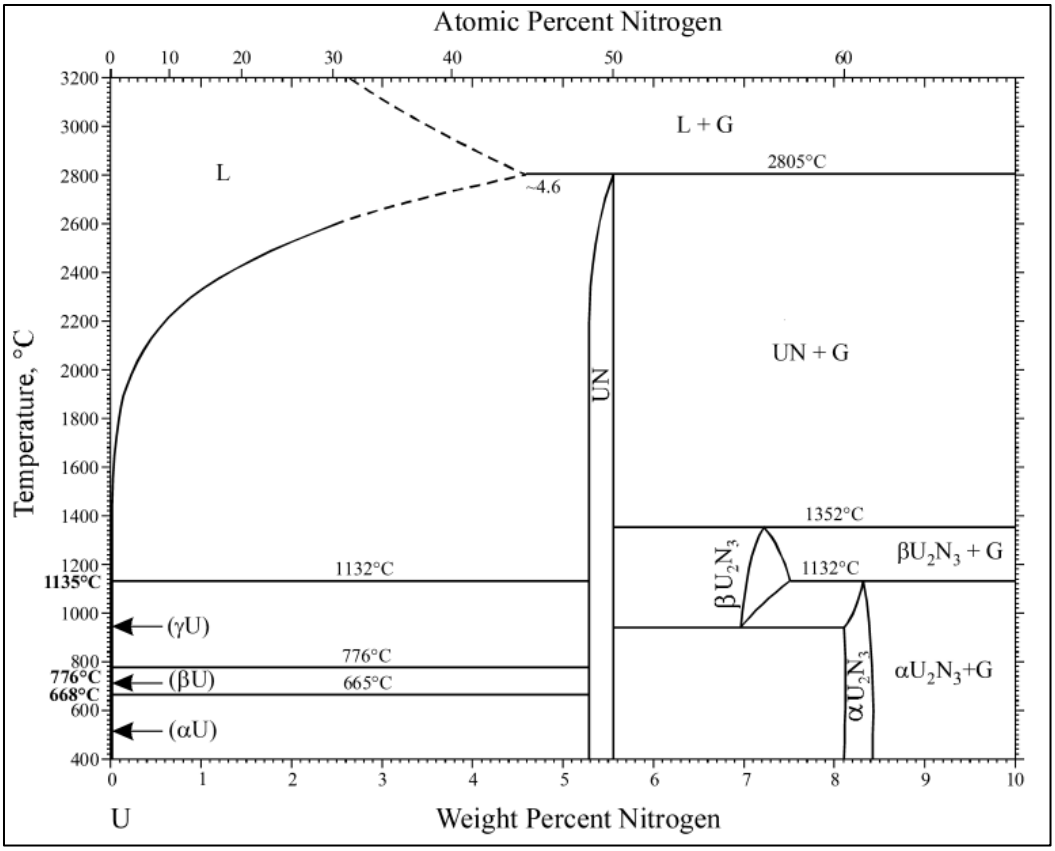

Figure 4.6: U-N phase diagram developed by Okamato et al. [25]

Micrographs from the samplings of atomized U-10Mo feedstock, U-10Mo milled for 40 hours (both 2- and 3-mm media), and 10 hours were obtained on a JSM-IT500HR scanning electron microscope. These micrographs are shown in Figure 4.7, and no bulk UN or U_2N_3 phases was observed within the microstructure using SEM/EDS techniques, despite appearing in XRD.

4.3.2 Particle Sizing Effect during Milling

Powder samples of 10 g each were milled as a function of time, number of nitrogen pressure regenerations, and media size. Average particle size for several of the milled batches are recorded in Table 4-3 and complimented by SEM micrographs and XRD patterns of select milled powders. Media size difference between 3 mm and 2 mm seemed to have little to no effect on resultant particle size. Milling times on the other hand seemed to have effects on particle size, with the greatest particle size reduction of nearly 50 μm being seen after 40 hours of milling. The atomized U-10Mo powder was found to have an average particle size of ~190 μm based on SEM micrographs, and was irregular in shape, with both spherical and

elongated particulates, similar to that of the atomized powder. This is hypothesized to be due to the SS media not having enough kinetic energy at 400 rpm to sufficiently deform U-10Mo, even after 64 hours. The U-10Mo chemical distribution was still homogenously distributed after atomization (Figure 4.7).

Table 4-3: U-10Mo particle size as a function of milling time.

Milling Time (hours)	**Average Powder Particle Size (μm) ***
0 (Atomized)	190
10	155
40	140
64 **	182

** Powder sizing was done by manually averaging the cross sections of at least 30 particulates.*
*** Total milling time; this is for the 40-hour sample milled with 2 mm media after a 24-hour mill with 3 mm media.*

4.3.3 Iron Contamination in Milled Material

Substantial iron contamination was noted in the samples milled for 10, 40, and 64 hours. It is hypothesized that this iron contamination is a result of the stainless-steel media and jar. The iron did not appear to alloy with the U-10Mo based on SEM and XRD micrographs shown in Figures 4.7 and 4.8, but instead formed a shell around the particulates. The iron shell thickness was seen in the tens of microns range. Fe and Cr contamination was quantified using an inductively coupled plasma – optical emission spectrometer (ICP-OES) and was found to be present within the 40-hour milled samples at 88,500 μg/g (32.85 at%) and 13,700 μg/g respectively (5.46 at%). To reduce the iron contamination, milling time was reduced, and iron contamination was gauged by Fe layer thickness on the outside of the U-10Mo particles for the 10-hour milled powder. Based on the micrographs shown in Figure 4.7, substantial Fe layering did not begin until sometime between 10-and 40-hours of milling but was observable by TEM and APT methods as early as 10-hours.

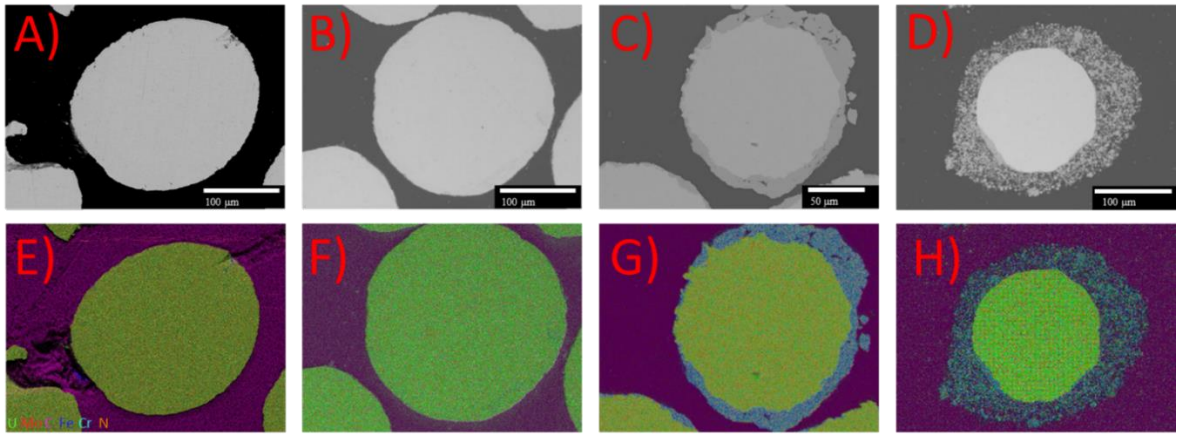

Figure 4.7: Backscatter SEM micrographs for atomized, 10-hour, 40-hour, and 64-hour (40 hour with 2 mm media) (A-D) complemented by EDS maps (E-H). Uranium/molybdenum distribution remains homogenous across milling times and media sizes. Fe contamination shell attributed to the stainless-steel milling media can be noted in the 40- and 64-hour milled powders, while the Fe and Cr contamination remains evenly distributed across the particulates in the 10-hour milled sample. Color key applies to all EDS maps.

Based on the locations of iron contamination, it was later predicted that most of the formation sites for nitrides would be on the outer surfaces of the powders, as breakup and welding together of powder fragments did not occur under these testing conditions, which means that the more stable nitrides would form in nanoparticles with the uranium first at the edge, followed by an iron nitride then molybdenum nitride. Minor uranium oxides would also be expected due to the presence of oxygen in ranges between <0.1-50 ppm in the argon glovebox in which these were prepared. Further details on the nitride and oxide formations may be found in sections 4.3.5 and 4.3.6.

4.3.4 Thermal Treatment Effects on UN Stabilization and Crystallinity

The 40-hour milled powder (3 mm) that was heat treated at 700 ℃ for 2 hours did not show the BCC γ-phase but yielded a combined UN and BCC-Fe phase. This aligns with TEM and APT data showing (Figures 4.16 and 4.17) that during the heat-treatment, the previously amorphous iron was recrystallized, and the UN nanoparticles either grew or agglomerated towards the surface of the powder. It is suspected that U-Mo is absent from the XRD pattern in Figure 4.8 due to the probe depth of X-Rays in U-10Mo only being 1.5-3.5 µm deep via MAC calculation. This was performed assuming a 0.75% packing factor and 17.2 g/cc density. With such a low probe depth, and with the large amount of both UN and Fe contamination residing almost exclusively at the surface of the powder particles, it makes sense that the γ-U phase would be difficult to resolve.

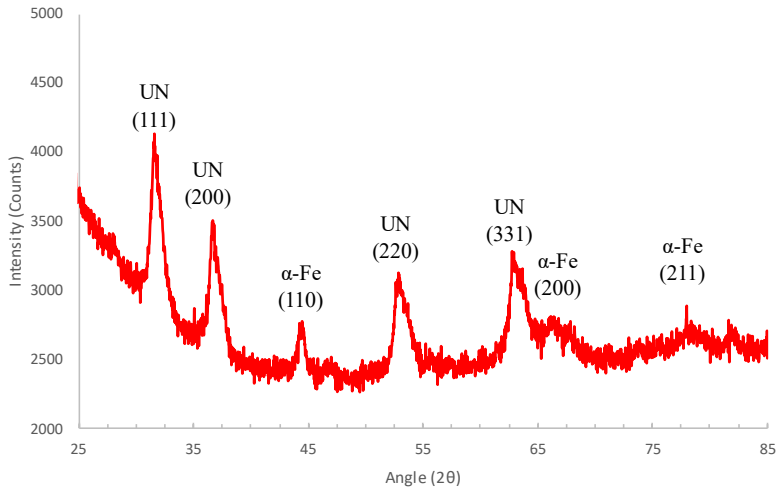

Figure 4.8: XRD pattern for heat-treated U-10Mo at 700 °C for 2 hours. Peaks indexed using Highscore Plus. Heat-treatment revealed the recrystallization of the ferritic iron on the surface of the powder, as well as migration or agglomeration of UN at the surface of the powder U-10Mo.

The heat treatment did not appear to have any kind of stabilizing effect on the UN phase, as the UN phase was already present and stable within the fuel as is shown via APT (Figures 4.18,4.19, and 4.21). No supplementary SEM imagery was gathered to further characterize the need for a heat-treating process.

4.3.5 UN Nanostructuring in U-10Mo Powder

***4.3.5.1** Microstructural Results via Transmission Electron Microscopy*

The primary characterization purpose was to identify and locate UN nanoprecipitates, quantify their presence within the feedstock powder, and compare findings with the hypothesized size and structure of these nitride nanoprecipitates mentioned above. Richer and poorer uranium loading zones were noted across the lamellae, which could be due to the removal of uranium from the solid solution in forming nitride nanoprecipitates, but is expected to be the nature of γ-phase U-10Mo, based on micrographs seen in other literature. The amorphous iron layer was present on the surface of 40+ hour milled samples, but iron contamination was present in bulk within the meat of the fuel as early as 10 hours into the mechanical alloying process based on TEM results. The fine precipitation in Figure 4.9B are iron particles that worked their way into the fuel meat, which is verified in Figure 4.11.

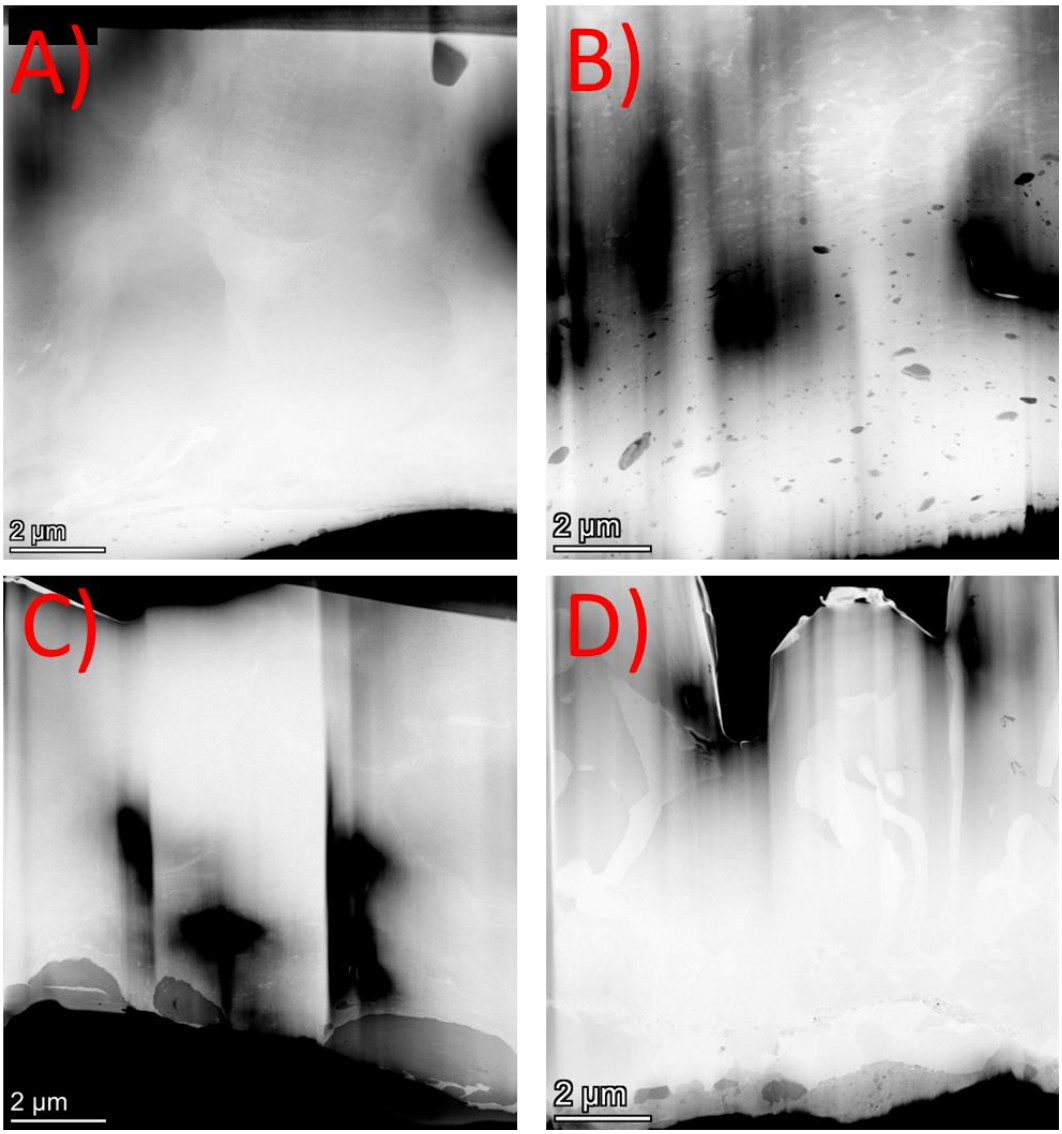

Figure 4.9: TEM micrographs of lamellae from the (A) 10-hour milled U-10Mo, (B) 20-hour milled U-10Mo, (C) 40-hour milled U-10Mo, and (D) 40-hour milled U-10Mo with 700 °C/2 hr. heat treatment. Dark grey speckles seen in (B) are iron contamination.

Upon closer inspection of the microstructures in each of these samples, dislocation pileups and high dislocation density in the grains was noted and is visualized in Figure 4.10. In addition to the amorphous iron agglomerate at the surface, this also contributed to reduced peak intensity seen in the XRD shown in Figure 4.5. This is an expected defect within the powder, as it has undergone extensive plastic deformation through the hours of planetary milling.

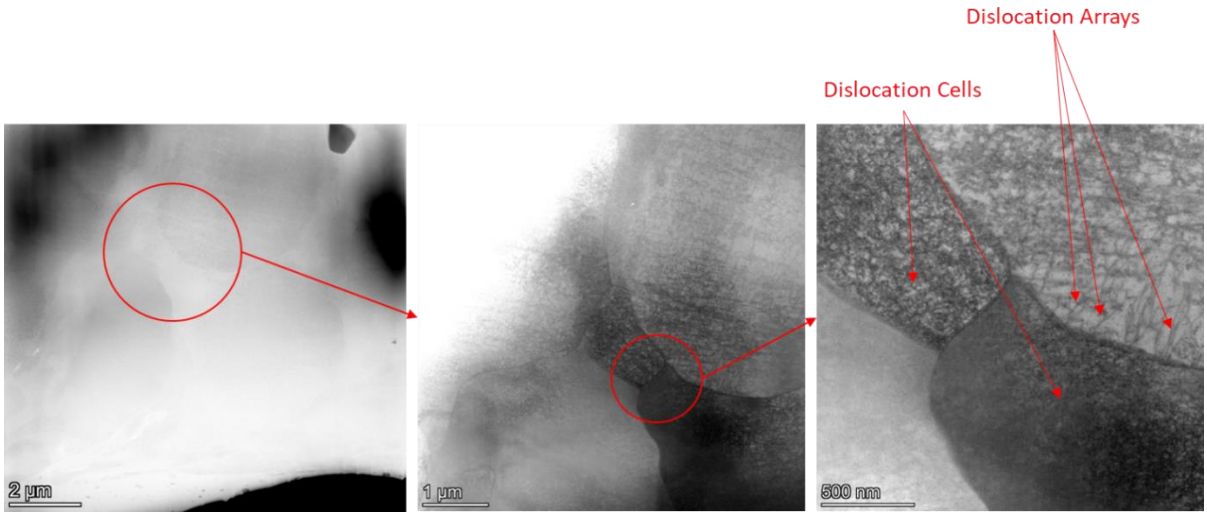

Figure 4.10: Dislocation cells and arrays as seen in U-10Mo milled for 10-hours.

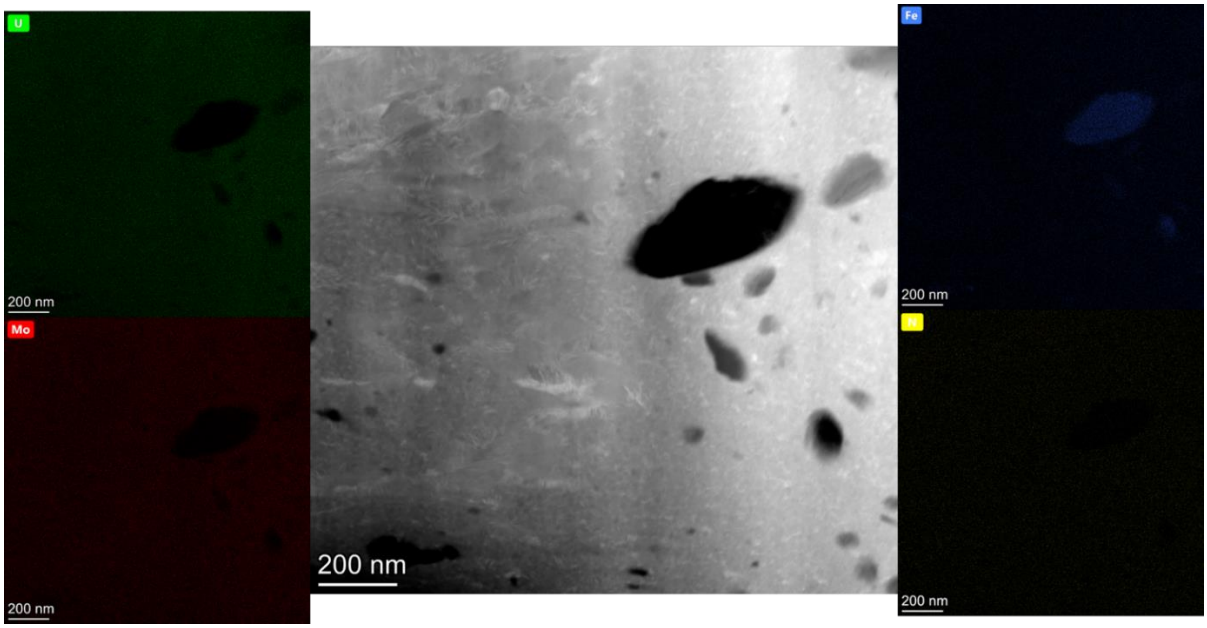

Figure 4.11: EDS maps of iron-contamination regions in 20-hour milled U-10Mo. Uranium and molybdenum contents still shown as being in solid-solution, while nitrogen is not seen in any meaningful quantities, and iron is rich in the dark grey and black speckled regions.

4.3.5.2 *Selected Area Electron Diffraction for Phase Verification*

Selected area electron diffraction (SAED) was used to try and pinpoint uranium nitride nanoparticles within the interior of the fuel, as well as verify the phase of material within the meat as well as the iron outer coating. Along the [111] plane SAED was conducted along the central U-10Mo material and revealed the characteristic BCC pattern of γ-phase U-10Mo, which is shown in Figure 4.12.

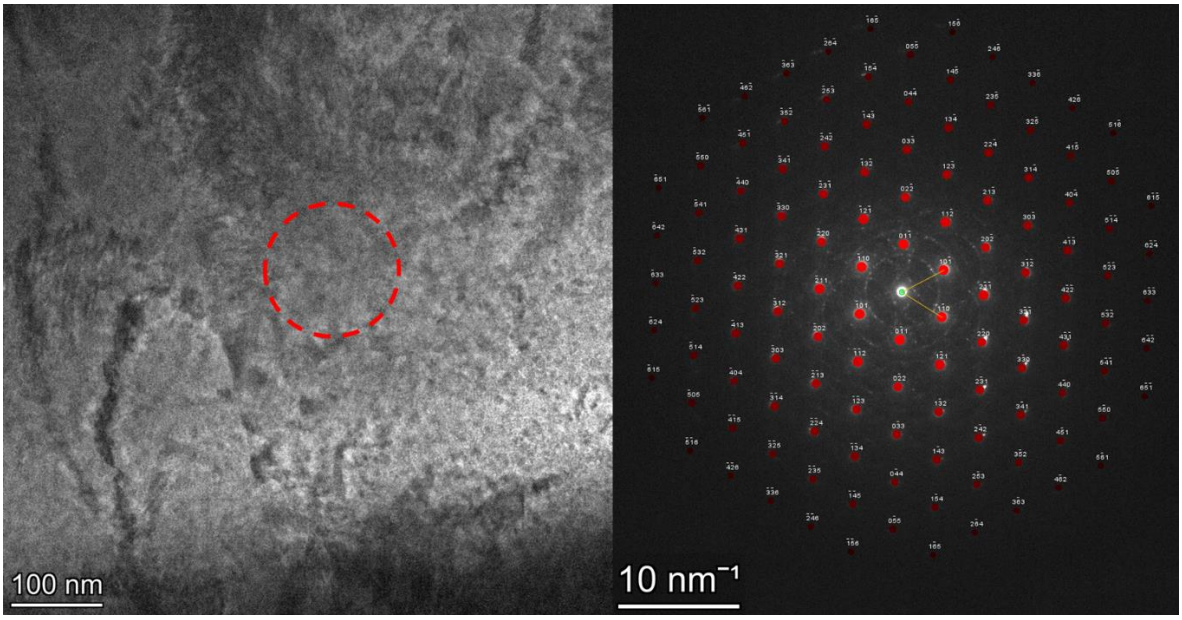

Figure 4.12: Indexed SAED pattern within the BCC U-10Mo along the [111] zone axis.

Within the peripheries of the 40-hour milled powder, the presence of amorphous iron was verified as well using SAED, with a characteristic amorphous ring being observed (Figure 4.13). This finding agreed with peak reduction noted in XRD data (Figure 4.5), as the mass attenuation coefficient (MAC) calculated probe depth for U-10Mo was 1.5 - 3.5 μm. This means much of the crystallinity within the U-10Mo was lost when trying to penetrate through the iron layer in the first place.

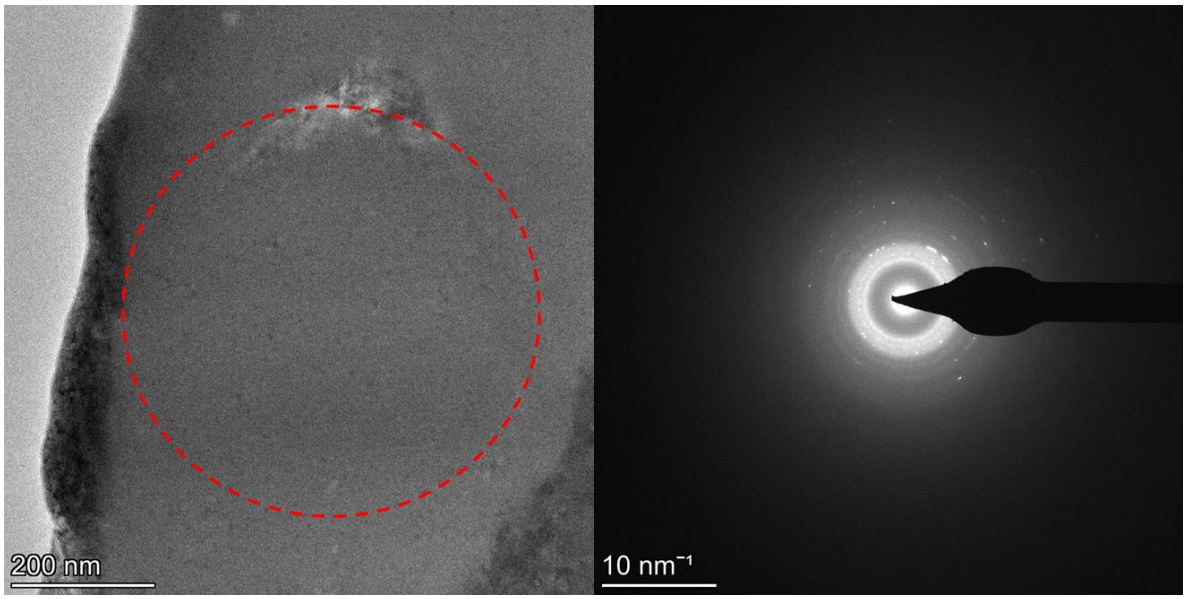

Figure 4.13: SAED pattern of amorphous iron encasing found on the outside of the 40-hour milled U-10Mo.

While a singular BCC phase was noted within the U-10Mo fuel meat, upon analyzing a broader area along the [001] zone axis, characteristic rings for a nanometric phase were observed, as seen in Figure 4.14. Upon indexing, the rings were found to correspond to UN, acting as an initial confirmation of nanometric UN being present within the fuel.

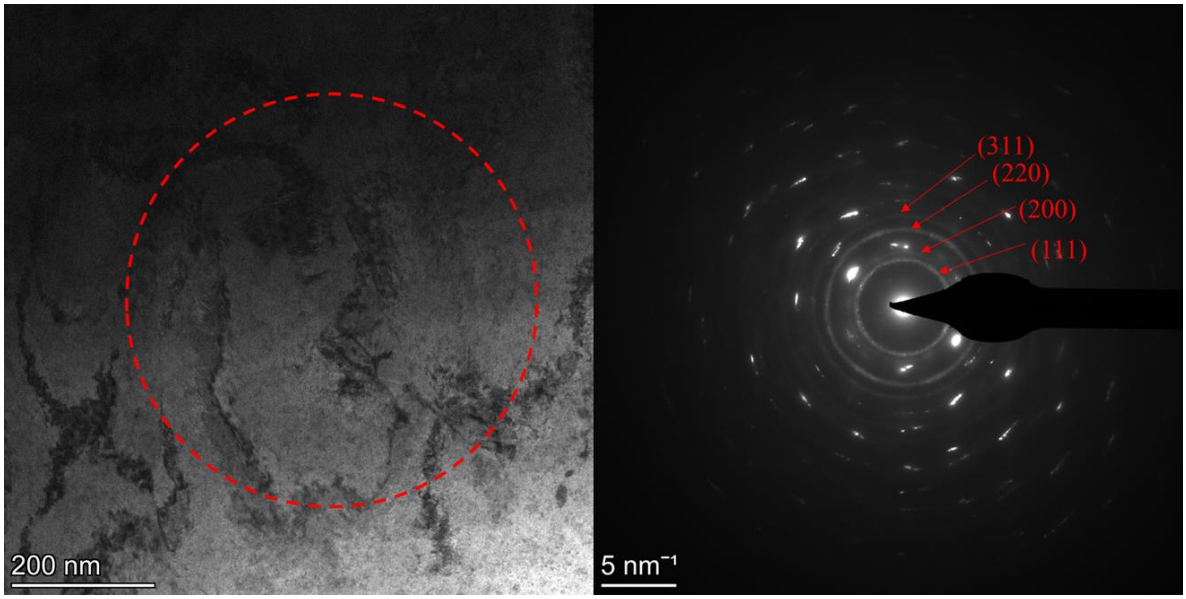

Figure 4.14: SAED pattern of U-10Mo fuel meat along the [001] zone axis. Indexed planes are those corresponding to a nanometric UN phase present within the matrix

4.3.5.3 *High-Resolution Transmission Electron Microscopy Results*

Utilizing ImageJ and techniques presented by Dr. K. Jeyadheepan [26], HRTEM micrographs were indexed to find the lattice parameter present within the U-10Mo fuel (Figure 4.15). Across 5 grains in the 40-hour milled material, the average lattice parameter was found to be 3.175 Å. According to Devaraj et al. at the Pacific Northwest National Laboratory (PNNL) the lattice parameter for γ-U-10Mo was measured at 3.41 Å using STEM methods [27]. This lattice parameter is 0.235 Å above this work's findings. The reasoning for this is hypothesized to be due to the nanocrystalline structure even found in the U-10Mo, driven by the mechanical alloying process. Other variable affecting the U-10Mo lattice parameter could be the extensive damage dealt to the lattice through mechanical alloying for 40 hours, or presence of solute elements. To prove any of these suppositions, SAED lattice parameter measurements would need to be made on the feedstock U-10Mo powder.

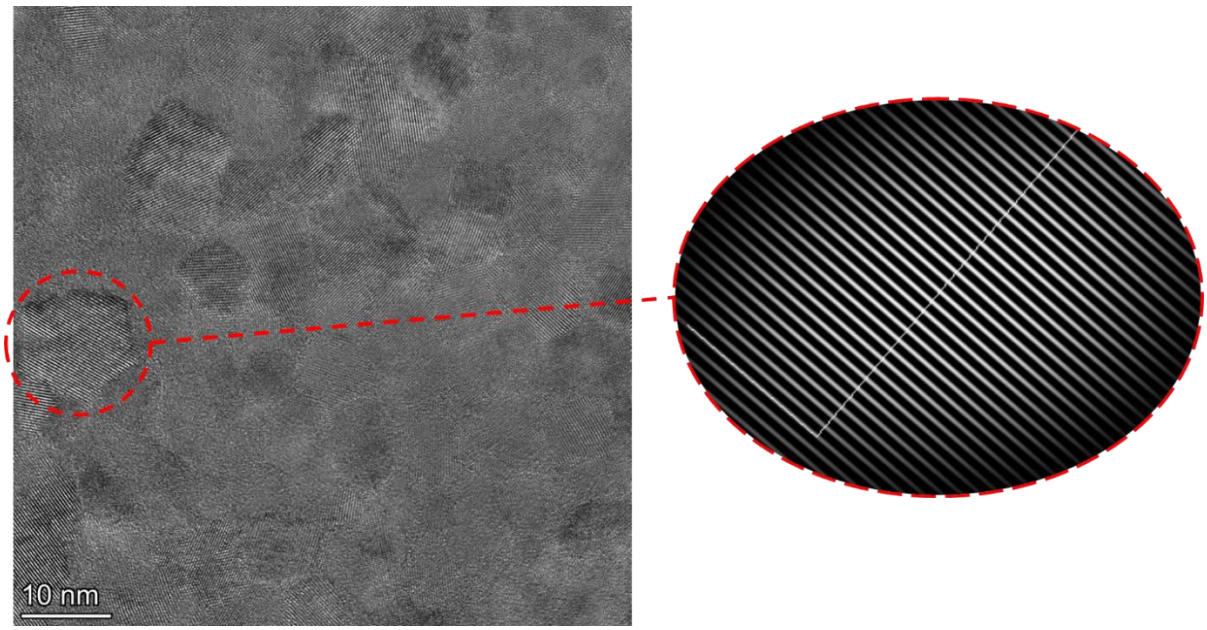

Figure 4.15: (Left) HRTEM micrograph of bulk U-10Mo matrix, revealing a nanocrystalline crystal structure, driven by the mechanical alloying process. (Right) Example of an indexed U-10Mo grain for lattice parameter determination through ImageJ utilization.

4.3.5.4 *Nitrogen Localization via Electron Energy Loss Spectroscopy*

In the heat-treated 40-hour milled U-10Mo, electron energy loss spectroscopy (EELS) analysis was conducted on agglomerated nano-crystallites observed at the periphery of the powder particles. Across multiple scans, upticks in nitrogen were observed across the nanoclusters of UN. This was one among the first pieces of evidence indicating a uranium nitride phase had been fabricated in the U-Mo fuel.

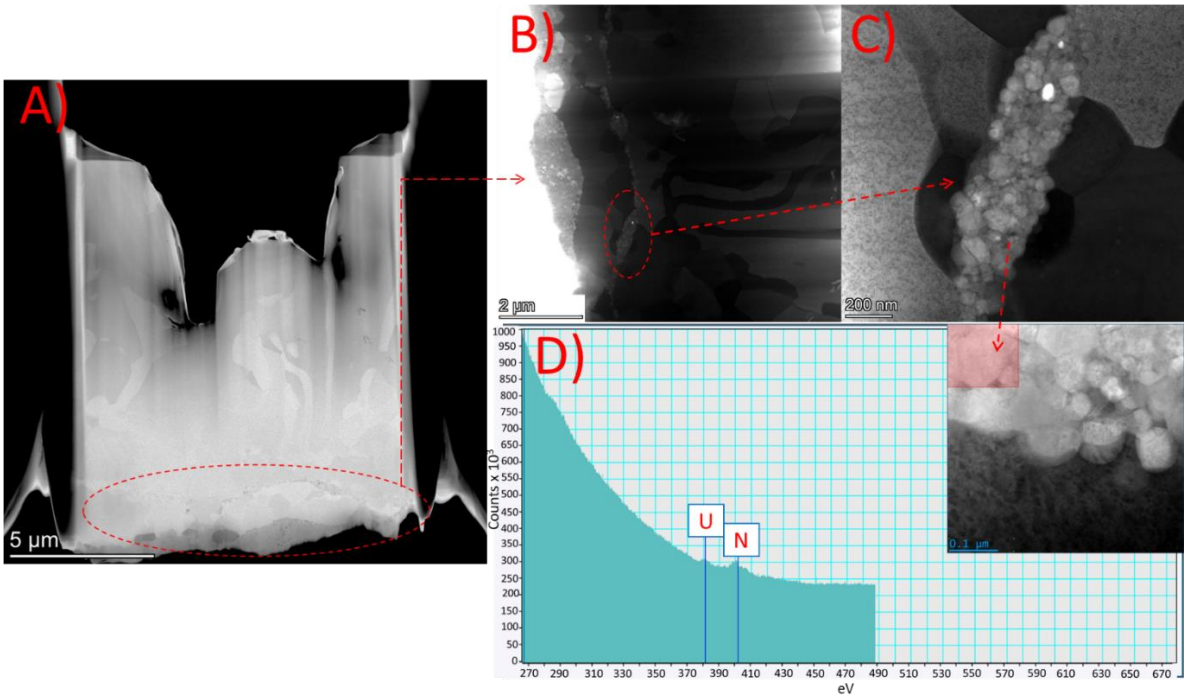

Figure 4.16: TEM lamellae taken from 40-hour milled and 2-hour heat treated U-10Mo powder, with outside face of powder facing down (A). Magnified image of edge region showing nanometric UN along periphery (B and C). EELS scan of a nanoparticle revealing the presence of both uranium and nitrogen (D)

These agglomerate regions were only observed in the heat treated 40-hour milled material. It is hypothesized that while the γ-phase recrystallized, the UN nanoparticles were pushed together by growing grains, causing them to be pushed together at the surface, but did not cause the nanocrystals to substantially grow due to UN's much higher recrystallization temperature.

4.3.5.5 *UN Nanocluster Morphology Results via Atom Probe Tomography*

In order to verify the supposition of UN being present within the U-Mo matrix found using EELS, APT needles were extracted from the 1-, 10-, and 40-hour milled (+700 ℃/ 2 hr. heat treat) U-10Mo powders to acquire high resolution compositional data on the nanometric regime. UN nanostructures were found in all three samples, with unique characteristics as a function of milling time and temperature. As shown in Figure 4.19, the 10-hour milled material had a distinguishable alloying region (region 1) that penetrated only about 200 nm into the U-10Mo powder. As seen in the green, the UN nanoparticles vary from 1-5 nm in radius, and are entirely limited to the iron contaminated region of the powder. Interestingly, UN was still the preferred compound formed in the amorphous iron, as shown by Figure

4.20, which shows the results of a composition scan across the UN nanoparticles produced in the 1- and 10-hour milled material.

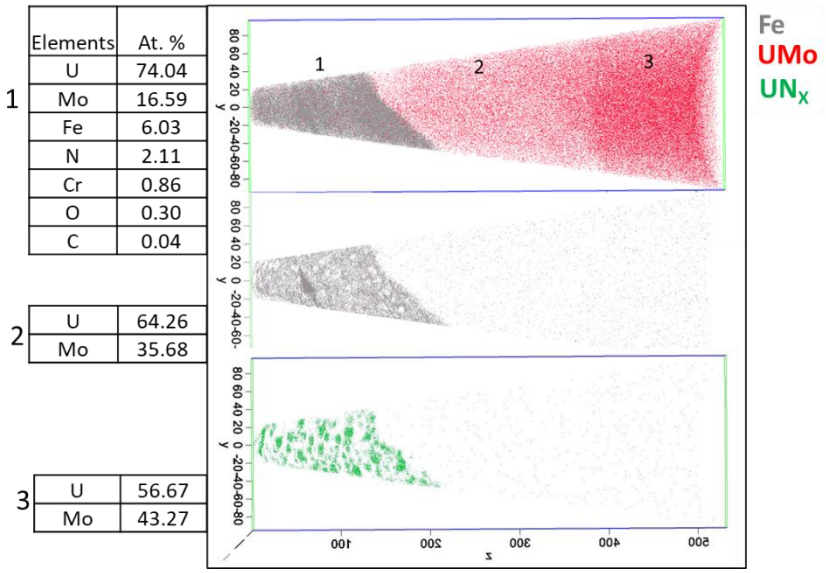

Figure 4.17: APT needle showing the concentration of atoms in each of three regions as well as a split-up showing iron and U-Mo overlay (top), iron presence by itself (middle), and UN nanoparticulates on their own (bottom). Alloying in this sample only occurred as deep as ~200 nm into the powder feedstocks. UN nanoparticles varied from 4-10 nm in diameter. Significant variation in U/Mo content occurred between region two and three. Sampling taken from U-10Mo alloyed for 10-hours

The content of molybdenum varied significantly as a function of depth into the powder particle. This could be a regional defect, as this behavior was not prominent across all samplings of milled U-10Mo but is likely due to the migration of uranium to form UN, and the presence of ferrite in the fuel system.

As a function of mill-time, nanoparticle size remained fairly constant, ranging primarily from 1-3 nm in radius in both the 1- and 10-hour milled material. Particle density on the other hand did increase with increased milling time, which is visualized in Figures 4.18 and 4.19. With a number density of $2.3 \times 10^{25} \frac{nanoparticles}{m^3}$ in the 1-hour milled material, and $2.7 \times 10^{25} \frac{nanoparticles}{m^3}$ in the 10-hour milled material, the increase in density was not drastic but does show a possibility in future milling experiments to control the total number of nanoparticles formed in the matrix, as well as derive an empirical equation for the number of UN sites as a function of milling time. It is likely that the number density of nanoparticles was limited by the small penetration depth into the actual fuel meat, which can be rectified in future research.

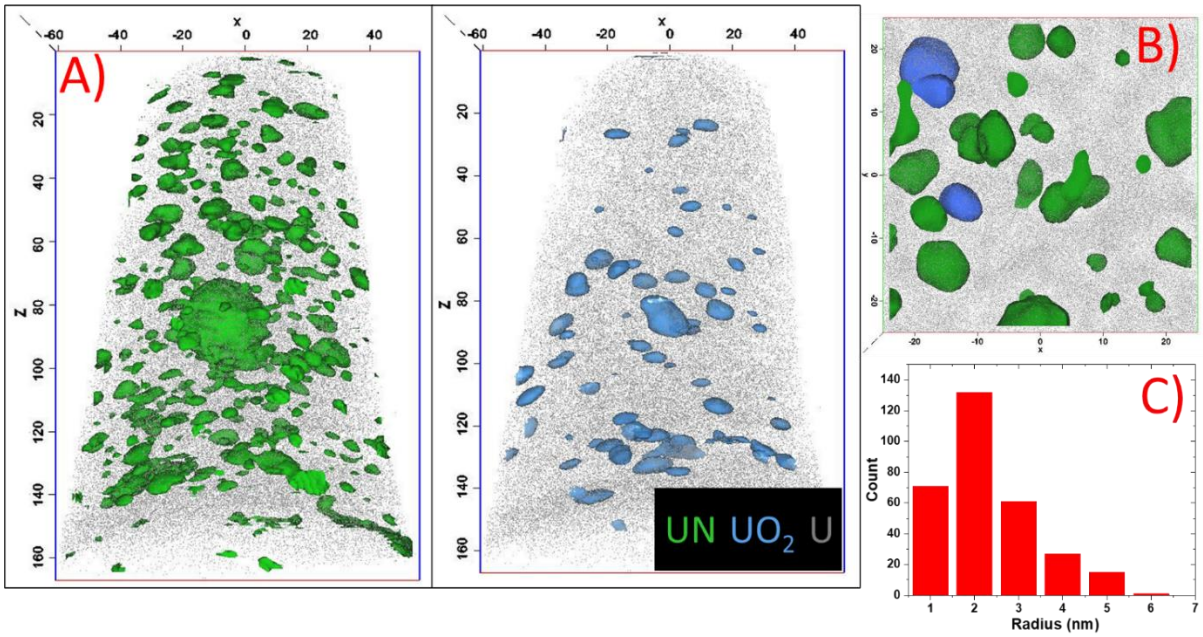

Figure 4.18: (A) UN and UO_2 distributed across a sample removed from the surface of the U-10Mo powder milled for 1 hour in 99.9995% pure nitrogen gas.(B) A 50x50x10 nm cross section revealing nanoparticle morphology in addition to the reduced uranium content surrounding the nanoparticles as seen by the lighter gradient around the UN and UO_2 sites. (C) Particle size distribution within the APT needle's volume. The majority of nanoparticles radii resided in the 2 nm range

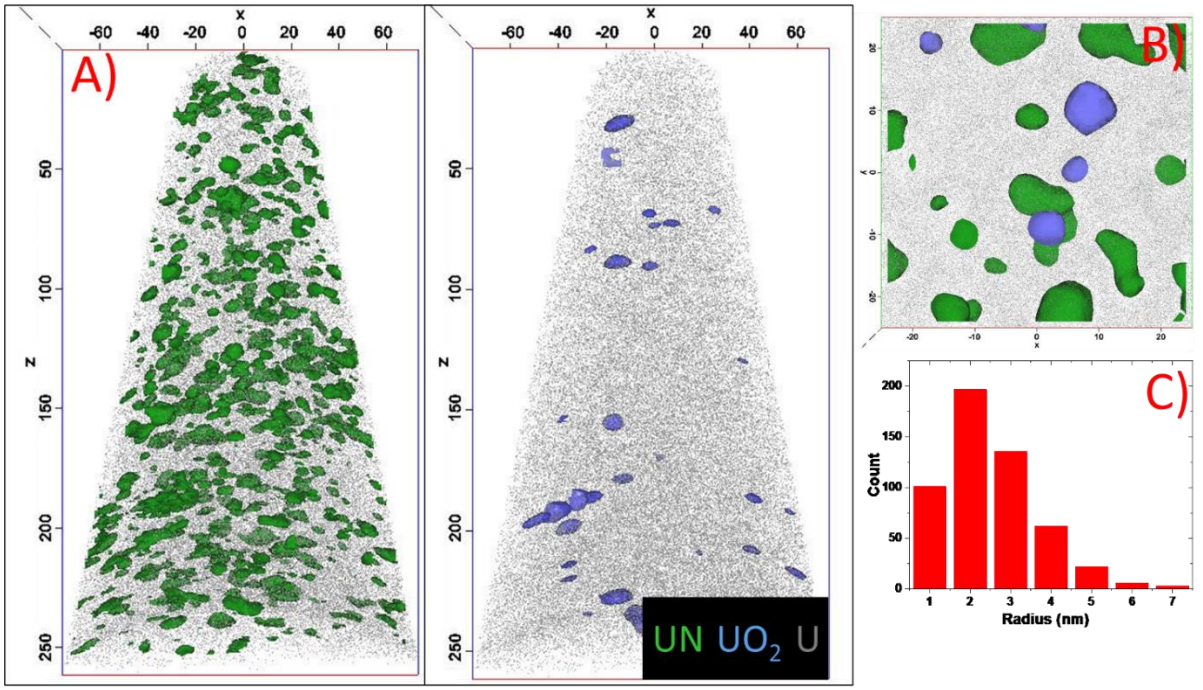

Figure 4.19 (A) UN and UO_2 distributed across a sample removed from the surface of the U-10Mo powder milled for 10 hours in nitrogen gas. (B) A 50x50x10 nm cross section revealing sample nanostructure. (C) Particle size distribution across the volume of the APT needle reveals that 2 nm radii particles are still the most common size.

A large agglomerate region of UN was also noted in the 1-hour milled U-10Mo. This could be a tight packed cluster of the UN nanoparticles, or an abnormality in the alloyed region, as

no other nanoparticles grew to that large of a size. Another peculiarity was the formation of uranium oxide nanoparticles within the outer 200 nm alloying region. These were formed in much smaller concentrations but remained distinct from the UN particles. These are hypothesized to be formed because of contaminant air in the nitrogen supply, or oxidized surfaces of the U-Mo or milling jar/media. For additional clarity on the contents of the UN nanoparticles, composition scans across UN from both the 1- and 10-hour milled U-10Mo are shown in Figure 4.20.

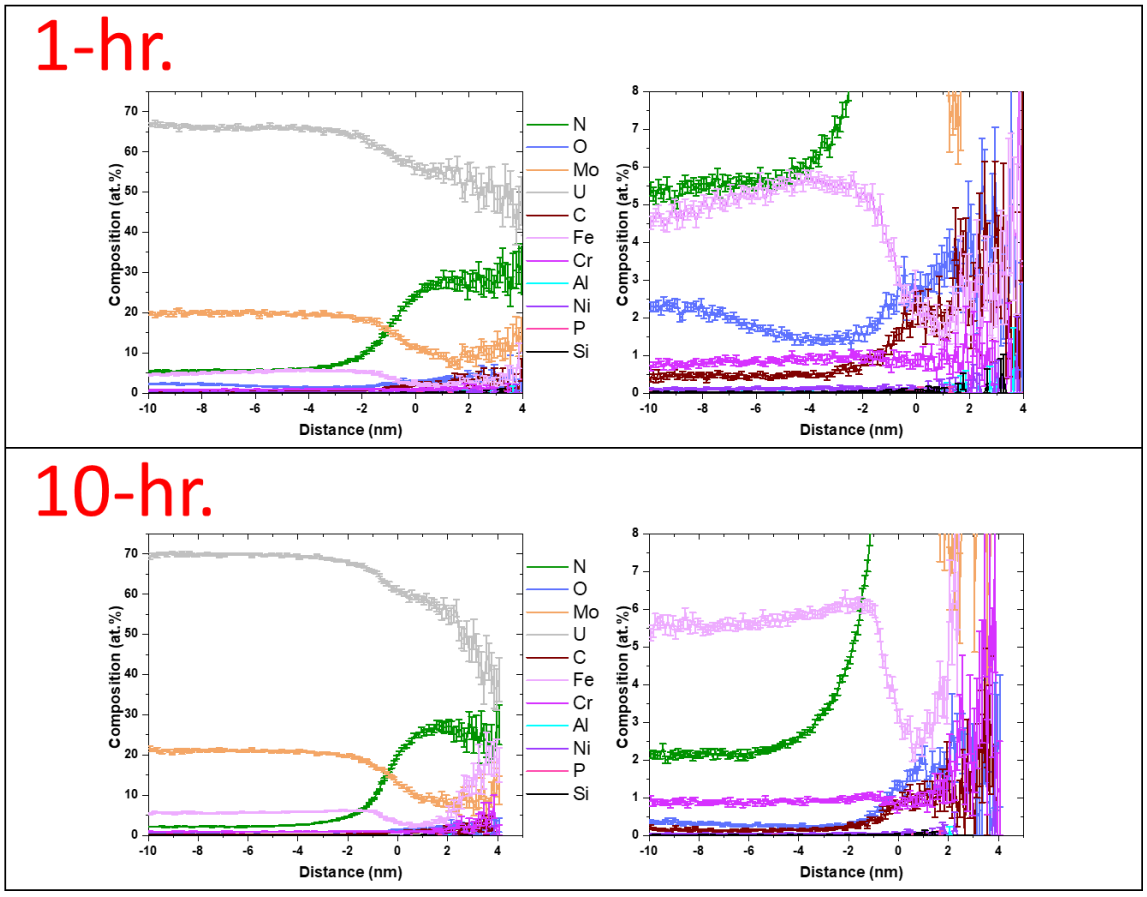

Figure 4.20: Composition scans taken across a UN nanoparticle from both the 1-hour milled (top) and 10-hour milled U-10Mo (bottom). Upon crossing into the UN phase, the uranium, molybdenum, and iron content drop, while the nitrogen increases greatly. Additionally, carbon and oxygen also increase slightly in the UN phase.

For the U-10Mo that was milled for 40 hours followed by the heat treatment, the nanoclusters of UN seen in the EELS section above were observed once more in the APT results, as a large UN agglomerate near the surface of the powder. Additionally, a uranium carbide (UC) phase was observed, indicating that as heat was applied to the system the carbon from the stainless steel interacted with the nanoparticles. The carbon also could have come from the

tube furnace which previously had trace amounts of grease on the edges of the ceramic tube, that was cleaned prior to use. This UC phase also had about 4 at% nitrogen in it, meaning that it could be a sub stoichiometric carbonitride phase, but this was not investigated further, since the heat-treatment of post-milled powder proved unnecessary and possibly detrimental to the distribution of nanoclusters within the U-Mo fuel.

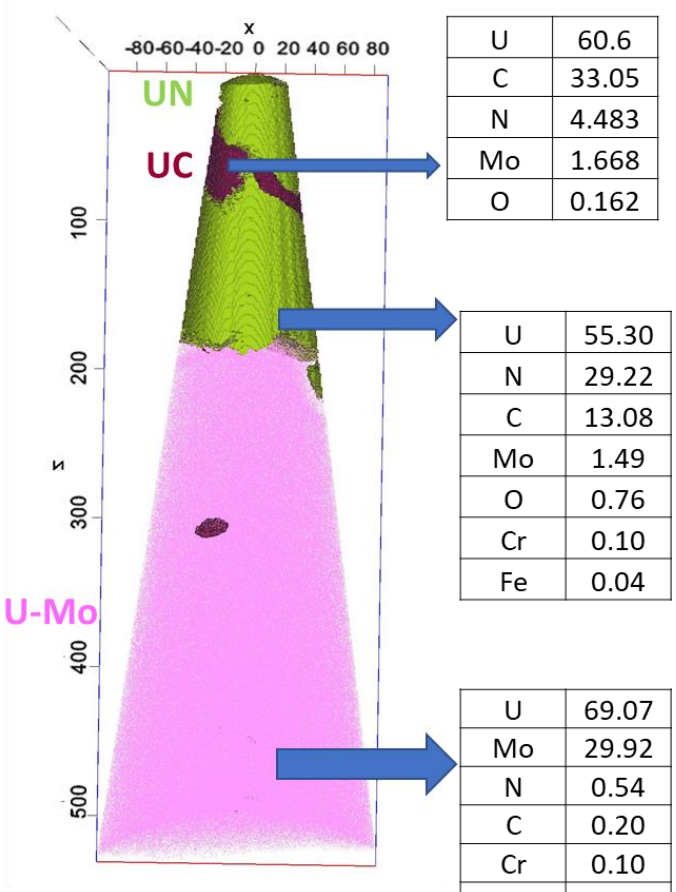

U	60.6
C	33.05
N	4.483
Mo	1.668
O	0.162

U	55.30
N	29.22
C	13.08
Mo	1.49
O	0.76
Cr	0.10
Fe	0.04

U	69.07
Mo	29.92
N	0.54
C	0.20
Cr	0.10
Fe	0.08
O	0.06

Figure 4.21: Sample removed from the 40-hour milled U-10Mo that was heat treated at 700 ˚C for 2 hours. A UN and UC phase were both present, and significant agglomeration of the secondary phases were found at the surface regions.

4.3.6 XRD and SEM Results from Spark Plasma Sintered U-10Mo/UN

The 1-hour milled material sintered successfully and yielded a density of 16.288 g/cc (94.7% theoretical density [%TD]) compact. The TD is based on the supposition that the amount of UN present within the system (~770 ppm, extrapolated from Figure 4.4) would not affect the overall density of the bulk U-10Mo compact. The sintered compact was cross sectioned, mounted in epoxy, and polished to a 1 µm finish and analyzed using SEM and XRD

techniques once more. The UN nanoclusters were observable even at lower magnifications and could be seen in “banded” formations around the edges of artifact U-Mo powder particles. This is proposed due to the distance between each of the bands of UN closely matching the size of the milled powder feedstock measured earlier. EDS revealed upticks in nitrogen across the banded regions which further assured the retention of the UN nanoclusters after spark plasma sintering.

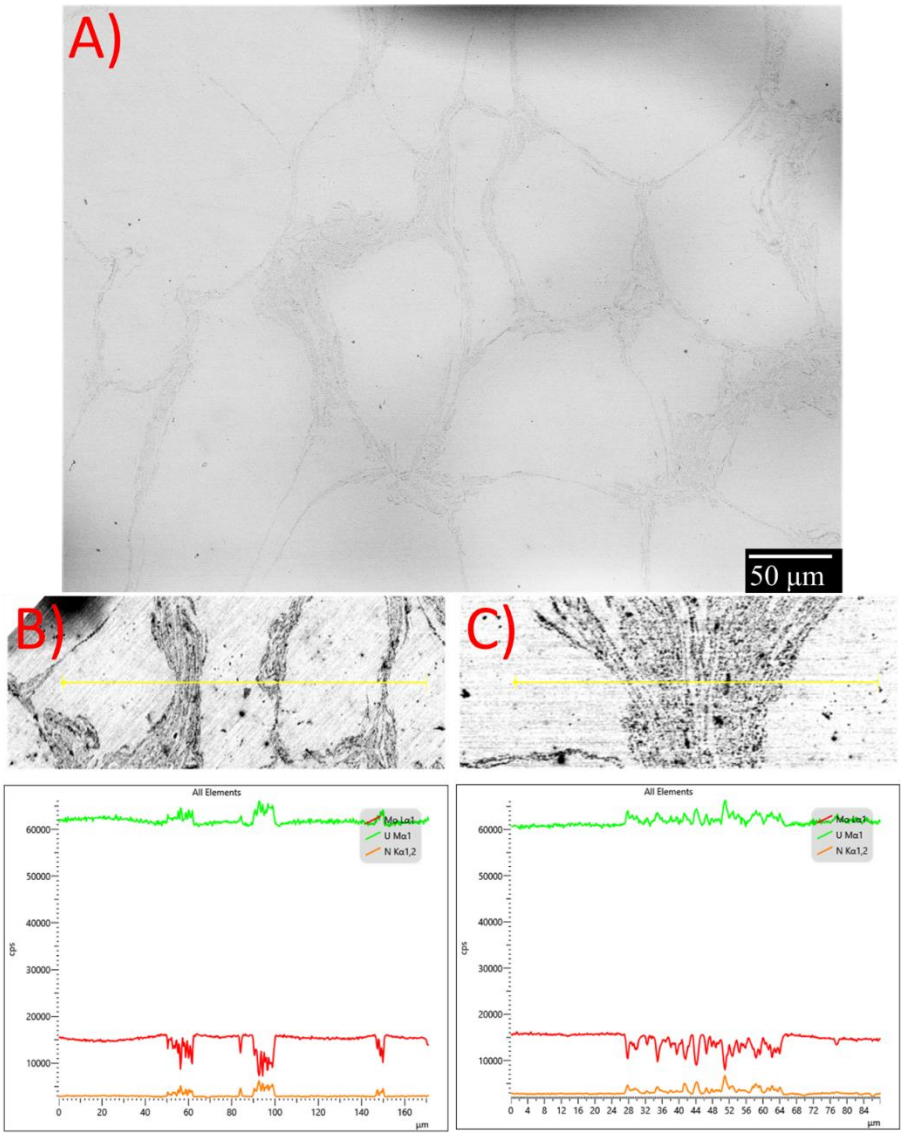

Figure 4.22: (A) SEM micrograph obtained from a cross section of 1-hr milled U-10Mo after field assisted sintering. The light grey region is γ-phase U-10Mo, and the dark grey bands are clusters of UN. (B) EDS linescan showing the decrease in Mo and increase in U and N when over the banded regions. (C) EDS linescan showing individual spikes for the uranium and nitrogen, indicating that these are not homogenous masses of UN but still in a nanostructured regime.

A high magnification backscatter SEM image shown in Figure 4.23 gives a general idea to the nanoparticle size, revealing UN sized on average ~180 nm. For precise measurements, TEM or APT analysis on the sintered compact would need completion in future work.

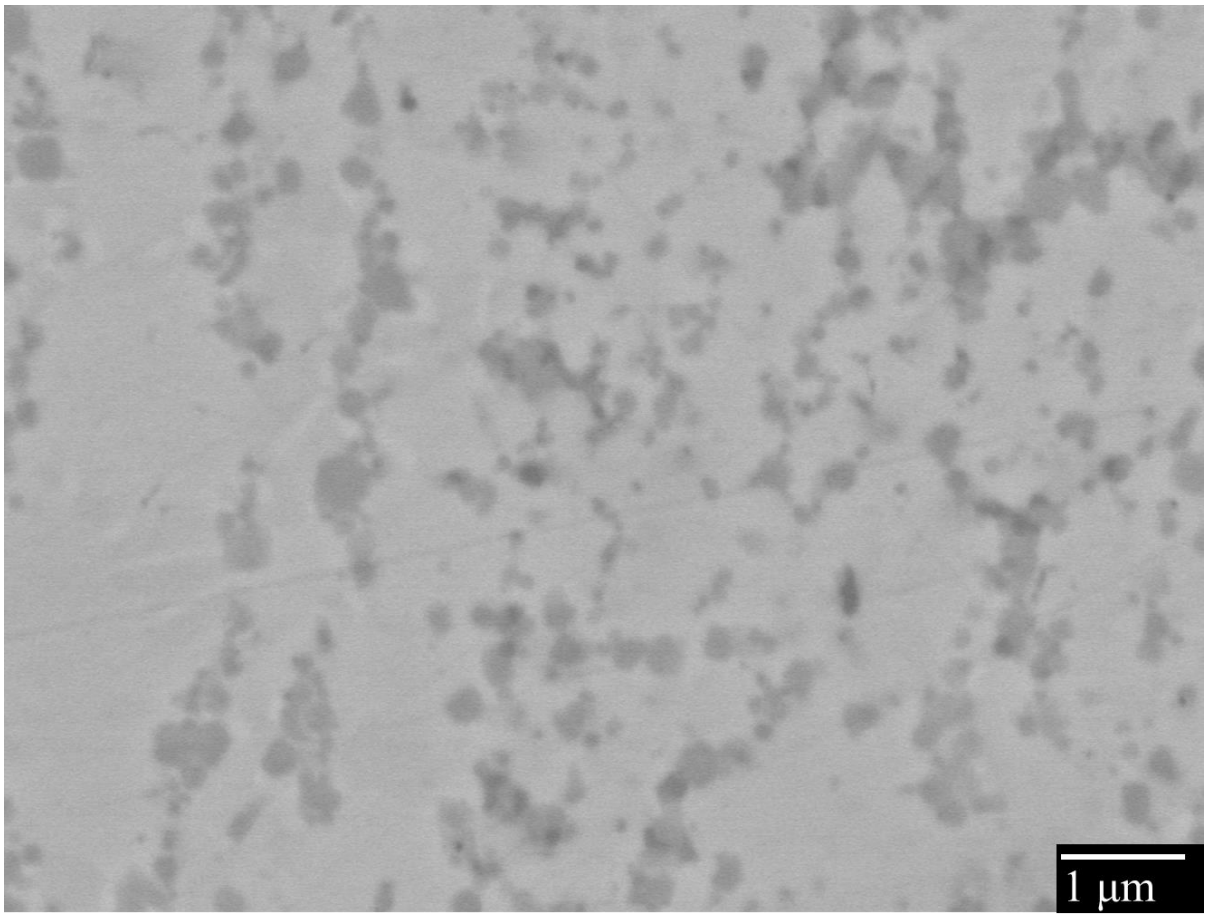

Figure 4.23: Backscatter SEM micrograph of UN nanoparticles at 13,000x.

When a piece of the same sintered compact was examined via XRD, the UN, γ-phase U-10Mo, and UO_2 phases were observed (Figure 4.24). The UO_2 phase was presumed to be due to oxidation during sample preparation but could also be due to the presence of oxide nanoclusters present within the alloy as well. The ICDD reference numbers for the γ-U-10Mo

phase, UN, and UO_2 phases utilized for this are 00-054-0495, 04-003-5402 and 01-071-4823 respectively.

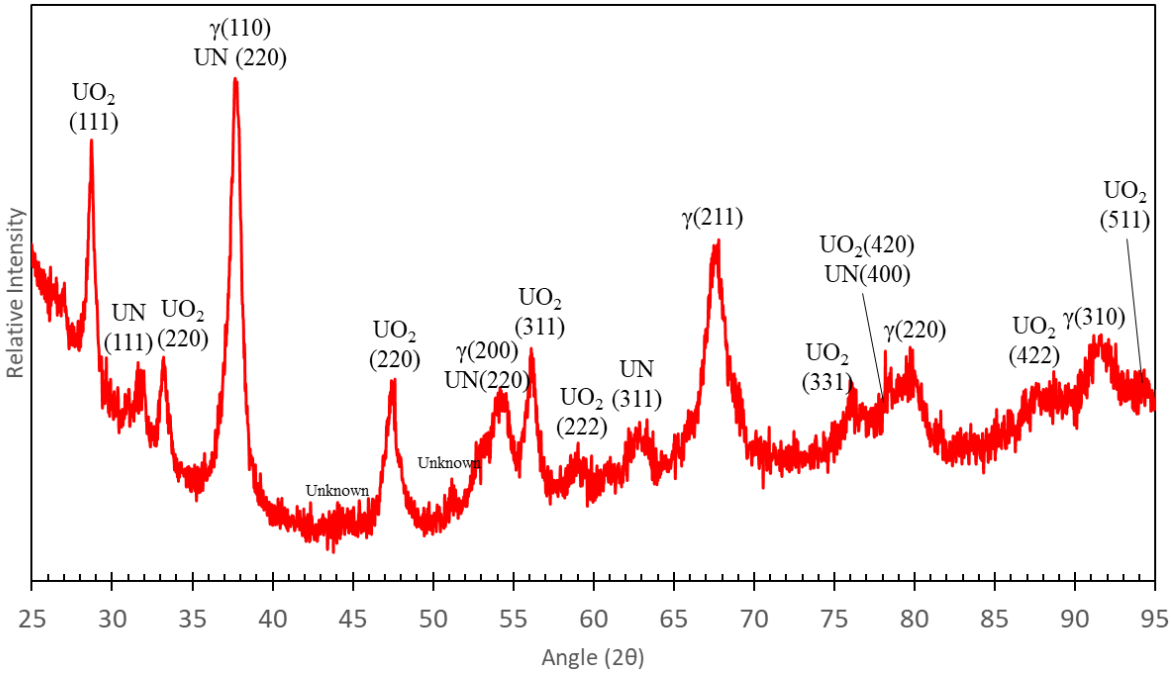

Figure 4.24: XRD plot of sintered 1-hr. milled U-10Mo. UO_2, UN, and γ-phase observed. The UO_2 phase could be due to oxidation after sample preparation, or possibly the UO_2 nanoparticles present within the clusters as seen in APT data.

The sampling of 40-hour milled material underwent a melt phase while sintering. This was presumed to be due to the high amount of iron present in the system after extended milling periods, as seen in Figures 4.5 and 4.7.

4.4 Conclusions

At the onset of this research, the fabrication of a homogenous UN nanostructure across a U-10Mo alloy was endeavored in an effort to address swelling due to fission products in the U-Mo system. The proposed method to achieve this was through mechanical alloying of a stabilized γ-phase U-10Mo powder in a 99.9995% pure nitrogen atmosphere for varying time periods.

The resultant powder had its light elements quantitatively analyzed, revealing an increase in nitrogen content within the alloy as a function of milling time, and hundreds of ppm of nitrogen being driven into the system by hour 10, and thousands of ppms of nitrogen present after 40 hours of milling.

The milled powders were also inspected using SEM, EDS, XRD, TEM, EELS, and APT methods. These methods showed:

1. Particle size of the milled powder does not decrease with increasing milling time due to the malleable nature of U-Mo, the insufficient impact rate or induced energy, and the deposition of stainless steel on the surfaces of the U-Mo particles.
2. Stainless steel deposited in an amorphous state due to the extensive damage to the crystal lattice during milling. This caused a reduction in XRD peak intensity as milling time increased. This was most noticeable at mill times ≥40 hours.
3. A secondary UN phase was indexed in the 10- and 20- hour milled material, showing that UN formed at earlier stages of the milling process meaning longer mill times were unnecessary to produce UN nanoclusters.
4. UN nanoclusters were observed in milled powders via TEM and APT methods. UN nanoparticles were 1-3 nm in radius. UO_2 nanoparticles were also observed but interspersed in smaller quantities. The UN and UO_2 nanoparticles were only found in clusters in the outer ~200 nm of the milled powders, presumably because that was the maximum achievable depth for alloying U-Mo with stainless steel media at room temperature.
5. EELS and SAED results showed additional proof in the amorphous iron layer, presence of UN nanoparticles, and formation of a nanocrystalline structure within the U-10Mo lattice as a whole.
6. Heat-treatment of milled U-10Mo at the recrystallization point (~700 ˚C) resulted in the agglomeration of nanoparticles into clusters at the edge of each powder particle. Presence of a UC phase was also observed near the surface of the heat-treated material.

After confirmation of the UN nanoclusters presence in the milled powders, the U-10Mo/UN powder that had been milled for 1- and 40-hours were spark plasma sintered. The 1-hour milled material successfully sintered, yielding a 94.7 %TD (16.288 g/cc) compact. Upon sintering under similar conditions, the 40-hour milled U-10Mo/UN allegedly melted due to the excess iron present creating a low-melting point U_6Fe phase. Upon inspection of the successfully sintered U-10Mo/UN using SEM techniques, UN nanoclusters were found in

bands surrounding where the artifact powder particulates resided prior to sintering. EDS was capable of picking up the change in uranium, molybdenum, and nitrogen content going across the banded regions. The XRD spectrum gathered from the sintered U-10Mo/UN revealed three phases, the BCC γ-phase of U-10Mo, UO_2, and UN. UO_2 is suspected due to oxidation of the sample or by presence of UO_2 nanoparticles presence within the alloyed material.

While not homogenously distributed within the U-Mo matrix, this work has shown that through mechanical alloying with a pure nitrogen cover gas, that UN nanoparticles of ≤10 nm can be created in a U-10Mo alloy in abundance, and that these nano-crystallites are chemically stable during heat-treatment and sintering processes but may be prone to diffusion into clusters at the edge of feedstock powders.

4.5 References

[1] A. Calka, "Formation of titanium and zirconium nitrides by mechanical alloying," *Applied Physics Letters,* vol. 59, no. 13, pp. 1568-1569, 1991, doi: 10.1063/1.106285.

[2] M. M. Cisneros, H. F. Lopez, H. Mancha, D. Vazquez, E. Valdes, G. Mendoza, and M. Mendez, "Development of austenitic nanostructures in high-nitrogen steel powders processed by mechanical alloying," (in English), *Metall Mater Trans A,* vol. 33, no. 7, pp. 2139-2144, Jul 2002, doi: DOI 10.1007/s11661-002-0045-1.

[3] S. Pasebani, "Processing of Oxide Dispersion Strengthened Alloys via Mechanical Alloying and Spark Plasma Sintering," PhD, Materials Science and Engineering, Materials Science and Engineering, University of Idaho, 2014.

[4] D. T. Hoelzer, "History and Outlook of ODS/NFA Ferritic Alloys for Nuclear Applications," *Transactions of the American Nuclear Society,* vol. 118, p. 4, June 17-21, 2018 2018.

[5] Z. F. Wu, L. D. Xu, H. Q. Chen, Y. X. Liang, J. L. Du, Y. F. Wang, S. L. Zhang, X. C. Cai, B. R. Sun, J. Zhang, T. D. Shen, J. Wang, and E. G. Fu, "Significant suppression of void swelling and irradiation hardening in a nanograined/nanoprecipitated 14YWT-ODS steel irradiated by helium ions," *J Nucl Mater,* vol. 559, p. 153418, 2022/02/01/ 2022, doi: https://doi.org/10.1016/j.jnucmat.2021.153418.

[6] M. P. Brady, J. A. Horton, P. F. Tortorelli, S. K. Wrobel, D. T. Hoelzer, E. A. Payzant, I. M. Anderson, and L. R. Walker, "Templated growth of complex nitride island dispersions by controlled internal reactions," (in English), *Abstr Pap Am Chem S,* vol. 223, pp. A83-A83, Apr 7 2002. [Online]. Available: <Go to ISI>://WOS:000176296800510.

[7] F. L. Oetting and J. M. Leitnaker, "The chemical thermodynamic properties of nuclear materials I. Uranium mononitride," *The Journal of Chemical Thermodynamics,* vol. 4, no. 2, pp. 199-211, 1972/03/01/ 1972, doi: https://doi.org/10.1016/0021-9614(72)90057-2.

[8] T. B. Lindemer, "Thermodynamic Factors Affecting UC1-xNx Irradiation and Synthesis," United States, 2005. [Online]. Available: https://www.osti.gov/biblio/885978

[9] J. H. Bartlett and A. Castro, "Isotopic spectroscopy of uranium atomic beams produced by thermal reduction of uranium compounds," *Spectrochimica Acta Part B: Atomic Spectroscopy,* vol. 155, pp. 61-66, 2019/05/01/ 2019, doi: https://doi.org/10.1016/j.sab.2019.03.011.

[10] G. De Micco, H. Nassini, and A. Bohé, "Kinetics of molybdenum oxidation between 375 and 500°C," 2014, pp. 313-338.

[11] K. Sabat, "Iron production by hydrogen plasma," *Journal of Physics: Conference Series,* vol. 1172, p. 012043, 03/01 2019, doi: 10.1088/1742-6596/1172/1/012043.

[12] F. Pomiro, J. Gaviria, A. Bohé, and G. De Micco, "Thermodynamic analysis of uranium oxides fluorination with HF(g) and F2(g)," *Journal of Radioanalytical and Nuclear Chemistry,* vol. 324, 04/27 2020, doi: 10.1007/s10967-020-07166-w.

[13] A. Vaucheret, R. Frédéric, Q. Jean, and A. Eric, "Determination of Gray Cast Iron Age Strengthening by Nondestructive Methods: Effect of Alloying Elements," *Journal of Materials Engineering and Performance,* vol. 28, 07/02 2019, doi: 10.1007/s11665-019-04180-2.

[14] S. L. Hayes, J. K. Thomas, and K. L. Peddicord, "Material property correlations for uranium mononitride: IV. Thermodynamic properties," *J Nucl Mater,* vol. 171, no. 2, pp. 300-318, 1990/05/01/ 1990, doi: https://doi.org/10.1016/0022-3115(90)90377-Y.
[15] A. K. Mukherjee and J. W. Martin, "Hardening of a molybdenum alloy by nitride dispersions," *Journal of the Less Common Metals,* vol. 2, no. 5, pp. 392-398, 1960/10/01/ 1960, doi: https://doi.org/10.1016/0022-5088(60)90048-5.
[16] W. E. Frazier, S. Hu, N. Overman, R. Prabhakaran, C. Lavender, and V. V. Joshi, "Recrystallization kinetics of cold-rolled U-10wt% Mo," *J Nucl Mater,* vol. 513, pp. 56-61, 2019/01/01/ 2019, doi: https://doi.org/10.1016/j.jnucmat.2018.10.046.
[17] "Microstructure Studies of Interdiffusion Behavior of U3Si2/Zircaloy-4 at 800 and 1000 C," 2017.
[18] R. L. Ludwig, "Low Alloy Additions of Iron, Silicon, and Aluminum to Uranium - A Literature Survey," Union Carbide, Oak Ridge Y-12 Plant, December 31, 1980 1980.
[19] J. Eckert, L. Schultz, and K. Urban, "Amorphization reaction during mechanical alloying: influence of the milling conditions," *J Mater Sci,* vol. 26, no. 2, pp. 441-446, 1991/01/01 1991, doi: 10.1007/BF00576540.
[20] D. Banerjee, "X-Ray Diffraction (XRD)," ed. Department of Chemical Engineering: IIT Kanpur.
[21] C. Suryanarayana, "Mechanical Alloying of Nanocrystalline Materials and Nanocomposites," *Madridge Journal of Nanotechnology & Nanoscience,* vol. 4, no. 1, pp. 127-134, 2019, doi: 10.18689/mjnn-1000126.
[22] S. Kirklin, J. E. Saal, B. Meredig, A. Thompson, J. W. Doak, M. Aykol, S. RÃ¼hl, and C. Wolverton, "The Open Quantum Materials Database (OQMD): assessing the accuracy of DFT formation energies," *npj Computational Materials,* vol. 1, no. 1, p. 15010, 2015/12/11 2015, doi: 10.1038/npjcompumats.2015.10.
[23] J. E. Saal, S. Kirklin, M. Aykol, B. Meredig, and C. Wolverton, "Materials Design and Discovery with High-Throughput Density Functional Theory: The Open Quantum Materials Database (OQMD)," *Jom-Us,* vol. 65, no. 11, pp. 1501-1509, 2013/11/01 2013, doi: 10.1007/s11837-013-0755-4.
[24] B. J. Jaques, B. M. Marx, A. S. Hamdy, and D. P. Butt, "Synthesis of uranium nitride by a mechanically induced gas-solid reaction," *J Nucl Mater,* vol. 381, no. 3, pp. 309-311, 2008/11/15/ 2008, doi: https://doi.org/10.1016/j.jnucmat.2008.07.043.
[25] "N (Nitrogen) Binary Alloy Phase Diagrams," in *Alloy Phase Diagrams*, vol. 3, H. Okamoto, M. E. Schlesinger, and E. M. Mueller Eds.: ASM International, 2016, p. 0.
[26] K. Jeyadheepan. "HRTEM d-spacing measurement." https://www.youtube.com/watch?v=uzClc-Cuz5s (accessed June 1, 2022).
[27] A. J. Devaraj, VV.; Manandhar, S.; Lavender, CA.; Kovarik, L.; Jana, S.; Arey, BW., "High-Resolution Characterization of UMo Alloy Microstructure," p. 26, November 2016.

CHAPTER 5

Concluding Remarks and Future Work

Conclusions

U-10 wt% Mo powder was created through an arc-melting/atomization process yielding a homogenous γ-phase alloy. Hydride-dehydride of U-10Mo was unsuccessful in this account but could be if material was heat-treated for longer to allow for the decomposition of the γ-phase into α- and γ'-phases that would more readily break apart when cycled under hydrogen. U-10Mo powder was successfully mechanically alloyed under a 99.9995% pure N_2 atmosphere, and successfully uptook nitrogen into the fuel, forming a nanometric UN phase. The majority of the nanoparticles were 1-3 nm in radii and were localized in the outer 200 nm of each of the U-Mo powder particles. Difference in milling media size (2 and 3 mm) showed no effect on resultant powder size after milling.

Powder that had been mechanically alloyed with nitrogen for 1 hour was successfully sintered using field assisted sintering techniques (FAST/SPS). The resultant compact reached a density of 16.288 g/cc (94.7 %TD) after sintering at 900 ˚C for 5 minutes under 40 MPa of pressure. UN nanoclusters were seen in bands across the entire cross section of the sample. The UN appeared to not diffuse during sintering and remain along the perimeters of the artifact U-10Mo powder particles.

Use of stainless-steel media yields substantial Fe contamination under prolonged milling in the U-10Mo system, causing X-ray fluorescence when using a Cu-kα source in X-ray diffractometry (XRD), which increases noise and impairs peak indexing.

Future Work

To drive the breakup of a ductile material like U-10Mo, a cryomilling setup would be suggested for future work. Additionally, work in measuring the post-sintered nanoparticles size and morphology within the U-Mo matrix is to be completed in the future. Hypothetically, the further the powder size is reduced in the U-10Mo feedstock, the more homogenously dispersed the nanoclusters of UN will be.

Utilization of lesser mill times, harder media (yttria-stabilized zirconia for example), reduced rpms, and use of a diffracted beam-monochromator are all being considered for future work with regard to iron contamination reduction and the quantification thereof.

Uranium nitride nanoclusters effectiveness in reducing fuel cladding chemical and mechanical interaction (FCCI and FCMI) still needs to be performed and is intended to be performed within the final year of the laboratory directed research and development (LDRD) funding. This will be tested by introducing simulant fission products like xenon and neodymium into sintered samples of U-10Mo with the embedded UN nanoclusters.